Active subglacial volcanism in West Antarctica

Running title: Active subglacial volcanism

Enrica Quartini[1,2†], Donald D. Blankenship[1] and Duncan A. Young[1*]

[1]*University of Texas Institute for Geophysics, Jackson School of Geosciences, University of Texas at Austin, Austin, Texas, USA;*

[2]*Department of Geological Sciences, Jackson School of Geosciences, University of Texas at Austin, Austin, Texas, USA;*

[†]*School of Earth and Atmospheric Sciences, Georgia Institute of Technology, Atlanta, GA, USA*

*Correspondence (duncan@ig.utexas.edu)

EQ, 0000-0001-7485-543X; DDB, 0000-0002-6866-8176; DAY, 0000-0002-6866-8176;

Abstract

A combination of aerogeophysics, seismic observations and direct observation from ice cores and subglacial sampling has revealed at least 21 sites under the West Antarctic Ice sheet consistent with active volcanism (where active is defined as volcanism that has interacted with the current manifestation of the West Antarctic Ice Sheet). Coverage of these datasets is heterogenous, potentially biasing the apparent distribution of these features. Also, the products of volcanic activity under thinner ice characterized by relatively fast flow are more prone to erosion and removal by the ice sheet, and therefore potentially underrepresented. Unsurprisingly, the sites of active subglacial volcanism we have identified often overlap with areas of relatively thick ice and slow ice surface flow, both of which are critical conditions for the preservation of volcanic records. Overall, we find the majority of active subglacial volcanic sites in West Antarctica concentrate strongly along the crustal thickness gradients bounding the central West Antarctic Rift System, complemented by intra-rift sites associated with the Amundsen Sea to Siple Coast lithospheric transition.

Preserved within the depths of the Antarctic ice sheet lies the record of past volcanic eruptions. This record gives us the unique capacity to understand the periodicity of volcanic eruptions at a continental scale, something rarely achieved in other terrestrial environments due to record loss from weathering and limited availability of written documentation.

Importantly, elevated geothermal flux associated with active volcanism can generate basal melt water that contributes to ice sheet instability by lubricating the base of the ice sheet and causing ice streams to speed up (*Pittard et al., 2016*). Basal water can facilitate sliding at the base of the ice in the area surrounding a heat anomaly and can also sustain subglacial hydraulic systems that lubricate the ice sheet further downstream (*Engelhardt, 2004b; Vogel & Tulaczyk, 2006*). Therefore, the effects of geothermal flux on ice sheet dynamics are not confined to the localized area of elevated heat flux. Through a combination of concentrated and distributed subglacial

water systems, melt water produced in regions of high geothermal flux is transported to distal areas (*Blankenship et al., 1993*). Thus, geothermal flux has the potential to indirectly enhance ice flow, and associated mass loss in coastal regions through the supply of upstream produced basal melt water.

In West Antarctica, the West Antarctic Ice Sheet (WAIS) is pinned to a number of subaerial volcanic edifices and subglacial mountain chains distributed throughout the region, but destabilized by the deep topographic trough of the West Antarctic Rift System (WARS, *Dalziel & Lawver, (2001)*). The WARS is a region of thinned, low lying continental crust mostly below sea level characterized by local mantle thermal anomalies (*Chaput et al., 2014; Lloyd et al., 2015*) and locally elevated geothermal flux (*Clow et al., 2012; Fisher et al., 2015; Schroeder et al., 2014*). WARS first extended in the Cretaceous (*Behrendt et al., 1991*), with subsidence and excavation through the Cenozoic (*Wilson & Luyendyk, 2009*), and subsequent local Neogene topographic enhancement (*LeMasurier, 2008*). Given the importance of geothermal heat flow and water to the stability of the WAIS, the potential threat that volcanism poses motivated extensive efforts to characterize subglacial active volcanism in West Antarctica (*Blankenship et al., 1993; Blankenship et al., 2001; Schroeder et al., 2014*).

Two aerogeophysical indicators have been used to argue for the existence of significant subglacial volcanism in the WARS: a large number of high-frequency (and thus shallow) circular magnetic anomalies observed from airborne magnetic data (*Behrendt, 1964, 2013; Behrendt et al., 1996*), and the identification of numerous 'cones' in bed elevation interpolations (*van Wyk de Vries et al. 2018)* derived from airborne radar sounding data (*Fretwell et al., 2013*). However, given the lack of direct sampling, understanding the interactions between active volcanism and the overlying ice sheet is key for understanding if these features are active.

In this paper we discuss the occurrence of active subglacial volcanism in the context of WAIS' glaciological regimes and WARS' geological and topographic structure. We show evidence that active volcanism beneath the WAIS occurs along crustal boundaries and regions of rifted, thinned crust, where local stress regimes allow for the upwelling of magma and hydrothermal fluids (e.g. *Maccaferri et al., 2014*). We also show evidence that active volcanism concentrates around regions of the WAIS that experience large fluctuations in ice thickness during glacial and interglacial cycles. There, changes in ice load can cause decompression melting and magma production in the underlying mantle, similar to what has been proposed for Greenland (*Stevens et al., 2016*).

We concentrate on subglacial active volcanism in West Antarctica due to the abundance of observations in this region. However, the approach to subglacial volcanism identification outlined for West Antarctica can be applied generally to other passive margins in Antarctica to begin a systematic search for similarly active subglacial volcanoes.

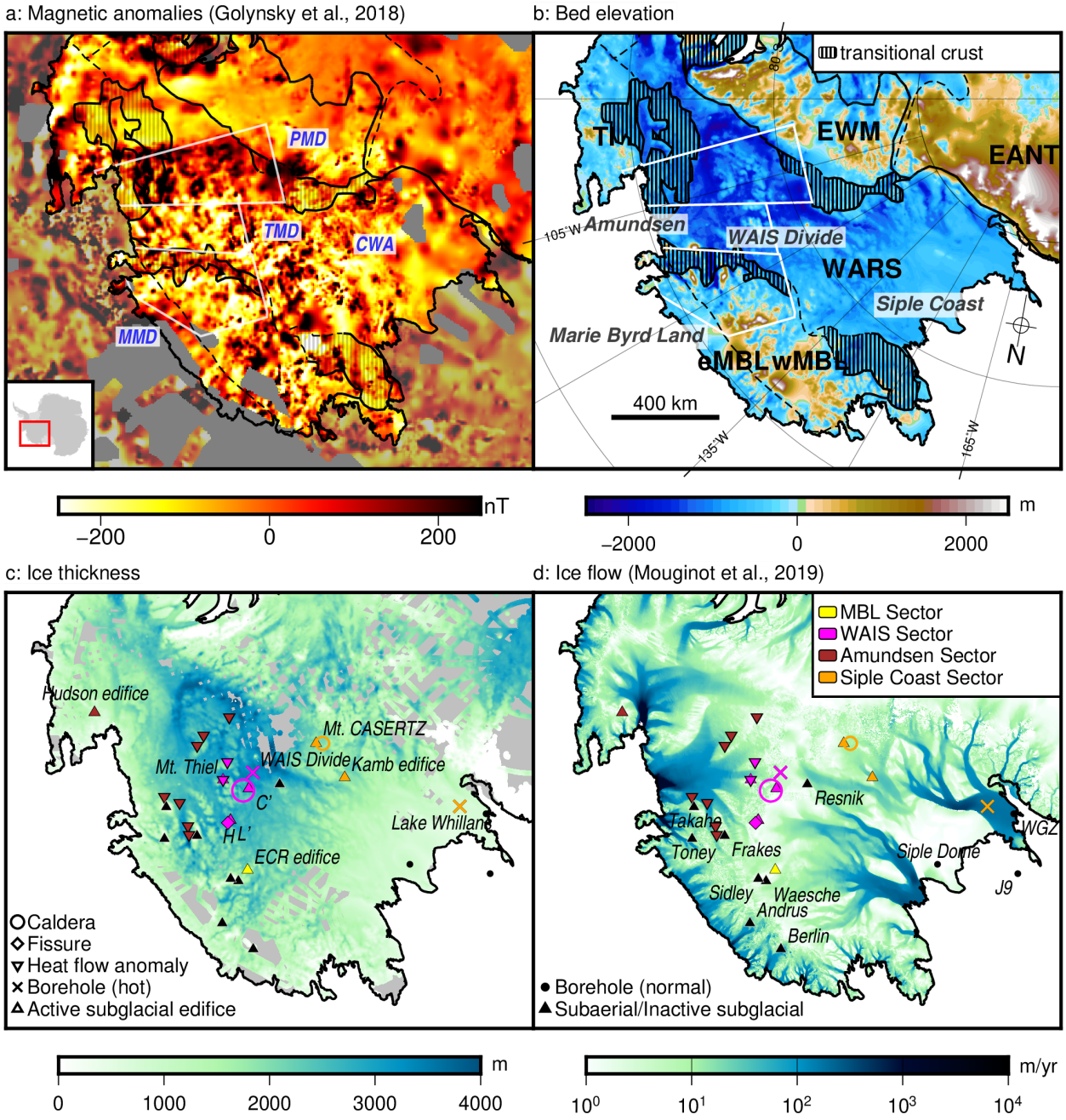

Figure 1: a) ADMAP2 magnetic anomalies (Golynsky et al., 2018). White lines outline boundaries between the Pine Island magnetic district (PMD), Thwaites Glacier magnetic district (TMD), and MBL magnetic district (MMD) (Quartini, 2018). Central West Antarctica (CWA) is also shown. b) Bedrock elevation combining data from (Blankenship et al., 2012; Leuschen & Allen, 2011; Vaughan et al., 2006; Young et al., 2017). Thick black lines outline crustal block margins and transition margins (Diehl, 2008): Thurston Island (TI), Ellsworth-Whitmore Mountains (EWM), eastern Marie Byrd Land (eMBL), western Marie Byrd Land (wMBL), East Antarctica (EANT), West Antarctic Rift System (WARS). Major sectors are shown. Distribution of volcanic features over c) ice thickness combining data from (Blankenship et al., 2012; Leuschen & Allen, 2011; Vaughan et al., 2006; Young et al., 2017); and d) ice surface velocity (Mouginot et al., 2019).

WARS geological context for subglacial volcanism

The lithospheric structure of West Antarctica determines key topographic, morphological, and thermal basal boundary conditions for the stability of the WAIS. Moreover, the lithosphere's influence on topography and structure may provide insight into the distribution of volcanism, which can occur where stress regimes facilitate the formation and emplacement of shallow-crustal magma chambers. *Paulsen & Wilson (2010)* examined these factors for West Antarctica's subaerial volcanoes. They found the age distribution of these volcanoes supports a connection between ice loading and unloading and periods of emplacement; however, the evolution of the distribution of subaerial volcanos in the highlands was controlled by changes in plate tectonic stresses.

Ice thickness and airborne gravity data reveal that West Antarctica consists of the WARS and five discrete microcontinental blocks characterized by distinct subglacial bed topography, crustal thickness, and gravity anomalies (*Dalziel & Lawver, 2001; Diehl, 2008*): the Ellsworth-Whitmore Mountains (EWM), Antarctic Peninsula (AP), Thurston Island (TI), eastern Marie Byrd Land (eMBL), and western Marie Byrd Land (wMBL) (Fig. 1 b).

Crustal block boundaries are interpreted from gravity anomalies. Bouguer gravity anomalies (which are corrected for the gravity signal of topography) primarily respond to the gravity signal from the crust-mantle interface, and are thus a proxy for crustal thickness. Sharp changes in Bouguer gravity indicate distinct crustal boundaries (Fig 1 b). Gradual changes in the Bouguer anomalies from positive to negative values indicate broad zones of crustal change and are interpreted as partially rifted transitional crust between crustal blocks and the rift zone (*Blankenship et al., (2001); Diehl, (2008),* Fig 1b).

Within West Antarctica, the WARS and Marie Byrd Land (MBL, composed of eMBL and wMBL, see Figure 1 b) are two regions identified as volcanically active. The WARS is a region of low bedrock topography and stretched continental crust (*Chaput et al., 2014; Fretwell et al., 2013*) characterized by a heterogeneous distribution of high geothermal flux (*Fisher et al., 2015; Schroeder et al., 2014*). Due to the low topography, large portions of central WAIS reside below sea level (up to – 2500 m), a highly unstable configuration susceptible to marine ice sheet instability, which can lead to runaway grounding line retreat and ice sheet collapse (*Schoof, 2007; Weertman, 1974*).

On the other hand MBL is an elevated plateau of high bed topography and thicker crust (*Chaput et al., 2014; Fretwell et al., 2013; LeMasurier, 2006*) sustained by a Cenozoic hot spot (*LeMasurier & Rex, 1989*) in the lower mantle beneath MBL, recently imaged by seismic tomography (*Accardo et al., 2014; An et al., 2015; Emry et al., 2015; Hansen et al., 2014; Heeszel et al., 2016; Lloyd et al., 2015*). Analysis of magnetic anomalies in eMBL shows evidence for multiple stages of tectonic reactivation in the mid-Cretaceous and support the hypothesis of a hotspot emplacement in the Miocene (*Quartini, 2018*).

Behrendt, 1964 found from International Geophysical Year era reconnaissance survey flights that northern West Antarctica is characterized by many high amplitude, but narrow magnetic anomalies, consistent with shallow volcanic rocks under the ice. The resolution increased markedly with the 5 km line spacing Corridor Aerogeophysics of the South Eastern Ross Transect Zone (CASERTZ) surveys of the 1990's (*Blankenship et al., 2001*). The CASERTZ data allowed Behrendt et al., 1996 to identify > 400 circular, small scale, high amplitude magnetic

anomalies in Central West Antartica (Fig. 1 a), interpreted as small scale intrusive bodies. In addition, *Behrendt et al., 1998* found evidence for large annular structures.

The Airborne Geophysical Survey of the Amundsen Embayment (AGASEA) project (*Holt, et al., 2006; Vaughan et al., 2006*) extended this magnetics coverage north with a 15 km grid. Using these data, *Quartini, 2018* found a contrasting suite of fabrics reflecting different lithospheric histories. In the WARS, different magnetic fabrics characterize the region adjacent to Pine Island Glacier (the Pine Island Magnetic District or PMD) and the center of Thwaites Glacier (the Thwaites Magnetic District or TMD). In PMD lies a region of very strong, large, annular anomalies, while in TMD a set of linear magnetic anomalies exist, paralleling similar features identified offshore in the Amundsen Sea and attributed to the mid-Cretaceous breakup of Antarctica (*Gohl et al., 2013*, Fig. 1 a). The circular small scale magnetic anomalies of Central West Antarctica are not apparent. On the other hand, under eMBL lies a region with suppressed magnetic fabric, with small scale, low amplitude magnetic anomalies (the MBL Magnetic District or MMD). The MMD and the TMD are separated by a continuous front of magnetic anomalies that corresponds well with the crustal boundary mapped from gravity by *Diehl et al., 2008* (Fig. 1 a and b). *Quartini, 2018's* interpretation was that the TMD represented older lithosphere not modified since the Cretaceous surrounded by younger rift and hotspot activity.

Vogel et al., 2006 found from dating subglacial samples along the Siple Coast that while there was evidence for petrologically mafic magmatism in West Antarctic, most of the dates obtained were Mesozoic ages, compatible with the primary rifting event. While this result appears to rule out pervasive contemporary volcanism as suggested by some interpretations of the magnetic data (*Behrendt et al., 1994*), it did not rule out local active volcanism.

WAIS glaciological context for subglacial volcanism

WAIS' ice dynamics and conditions at the bed impact both the type of volcanic products and their record of preservation. Glaciovolcanism has been well studied for ice thickness of < 800 m (*Gudmundsson et al., 1997; Smellie, 2000*) in Iceland. The WAIS has a much larger range in ice thicknesses (and hence pressure, Fig. 1 c) and ice flow speed (and hence erosional capacity *Behrendt et al., (1995)*; Fig. 1 d) relevant to understanding sites of subglacial volcanism. Given the importance of ice-magma interactions to subglacial volcanism, we describe both our approach for defining activity, and our framework for the variable response of volcanism to differing ice conditions.

The thermodynamic response of ice to pressure and temperature changes and the impact of melt water in subglacial environments introduce processes that extend the effect of volcanism both spatially and temporally. For this reason, we consider any subglacial volcanism that affects or has affected the current ice sheet as active. Based on the approximate minimum age of WAIS's oldest ice retrieved at the WAIS divide ice core site (*Buizert et al., 2015*) and the cooling rates of magma chambers (*Hawkesworth et al., 2000*) for compositions observed in West Antarctica (*LeMasurier & Rex, 1989*), we define the time interval of active subglacial volcanism in West Antarctica as the last ~ 100,000 years.

The main effect of subglacial volcanism is the rapid conversion of ice to water. For very thin ice (< 100 m), this process will rapidly breach the ice sheet, and the edifice will evolve to a subaerial style. For ice of the thickness seen in Iceland, an englacial vault of melt water can be generated, under a depression in the ice surface that will act to trap subglacial water (*Schmidt et al., (2011)* supplementary materials, *Smellie, (2000)*). Within the vault, the style of volcanism is subaqueous,

forming a pile of hyloclastite material and pillow lavas (*Gudmundsson et al., 1997*). Eventually, with sustained activity, this vault can breach the surface, causing a direct transition from a subaqueous mode to a subaerial mode, and leading for basaltic compositions to flat topped formations termed "tuya" or "table mountains" (*Smellie, 2006*).

At larger ice thicknesses, breaching becomes unlikely. In addition, the overburden pressure of the ice will force the collapse of englacial cavities through ice flow, although this process will be in tension with the hydraulic trapping of water by any surface depression (Fig. 2 a). Rapid ice flow will often correspond to inclined surface slopes and significant hydraulic gradients that will dominate water flow, which will serve to drain englacial vaults and suppress the formation of hyloclastite-pillow lava piles (Fig. 2 b). Eruptions under thick ice generate volcanic products typical of high pressure regimes such as lava sheets and pillow lava flows (Fig. 2 c). On the other hand, under shallower ice, volatiles in the magma expand allowing for faster quenching and breaking up of magma into mixtures of pillow lavas and hyaloclastite deposits.

Regions of fast ice flow are more efficient at removing volcanic deposits at the bed, especially poorly consolidated material such as hyaloclastites (*Behrendt et al., 1995*). We therefore expect subglacial volcanic products to be more easily removed along tributaries and ice streams and better preserved along ice divides (Fig 2).

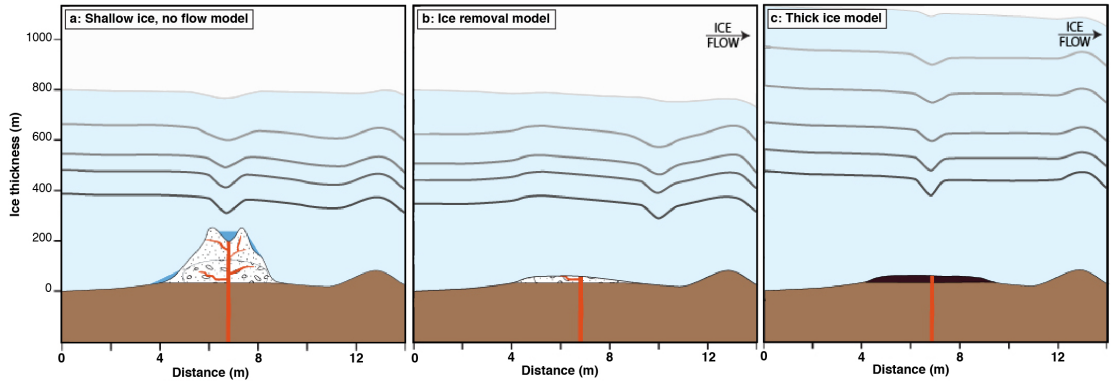

Figure 2: a) Shallow ice, no flow model: Subglacial volcanic edifice produced under shallow ice conditions, composed of poorly consolidated hyaloclastite atop pillow lava (Blankenship et al., 1993; Gudmundsson et al., 1997) and preserved due to slow to no ice flow; b) Shallow ice, fast flow model: effect of ice removal due to fast ice flow on a hyloclastite and pillow lava edifice (Nereson et al., 1998); c: Thick ice model: removal-resistant basaltic lava flow produced under thick ice sheets.

Techniques and observations

Direct observations of active subglacial volcanism are difficult to obtain due to the thick West Antarctic ice sheet cover (over 2500 m thick in places). First, thick ice sheets greatly attenuate the subglacial topographic signature that can be directly inferred from the ice surface. Secondly, the single-point nature of ice cores and boreholes make drilling efforts prohibitively expensive and overall inefficient at characterizing subglacial volcanic constructs.

In contrast, indirect observations from geophysical methods provide a more cost-effective way to characterize the internal structure and properties of both the ice sheet and the underlying bed topography. Geophysical surveys have the advantage of covering large areas at varying degrees

of spatial resolutions. Some of these methods include, but are not limited to, radar sounding, laser altimetry, potential fields, GPS, and passive seismic monitoring.

Identifying active subglacial volcanism requires multiple independent supporting evidence. While individual techniques can be used to identify plausible subglacial volcano candidates, it is the joint observations across different techniques and measurements that allows one to fully characterize each potential site of active subglacial volcanism. Here we will review some of the most common direct and indirect methods used to investigate active subglacial volcanism in West Antarctica.

Ice penetrating radar

Ice penetrating radar (IPR) transmits electromagnetic waves that travel through a medium, and detects changes in the dielectric permittivity of different materials by reflecting and refracting parts of their energy along each interface (*Gudmandsen, 1971*). The dielectric permittivity is a property of materials that depends on their composition, density, and structure. Therefore IPR can both detect the geometry and identify properties of subglacial interfaces. The larger the contrast in the dielectric permittivity of two continuous materials the stronger the IPR reflection, and the easier it is to identify the interfaces, also called radar reflectors.

IPR can be used to characterize the ice surface, bed topography, and englacial layers, which are caused by ash and aerosol products of volcanic eruptions that become incorporated in snowfall (*Fahnestock et al., 2001; Hindmarsh et al., 2006; Siegert et al., 2004*) and are interpreted to represent isochronous events recorded within the ice (*Whillans, 1976; Jacobel et al., 1993; Fujita et al., 1999*). Englacial radar layers are particularly useful as they allow geographical extension of the composition and age/depth record measured in ice cores over hundreds of square kilometers (e.g. *Cavitte et al., (2016)*). Evidence for active subglacial volcanism from IPR comes from interpretation of both the geometry and properties of radar interfaces.

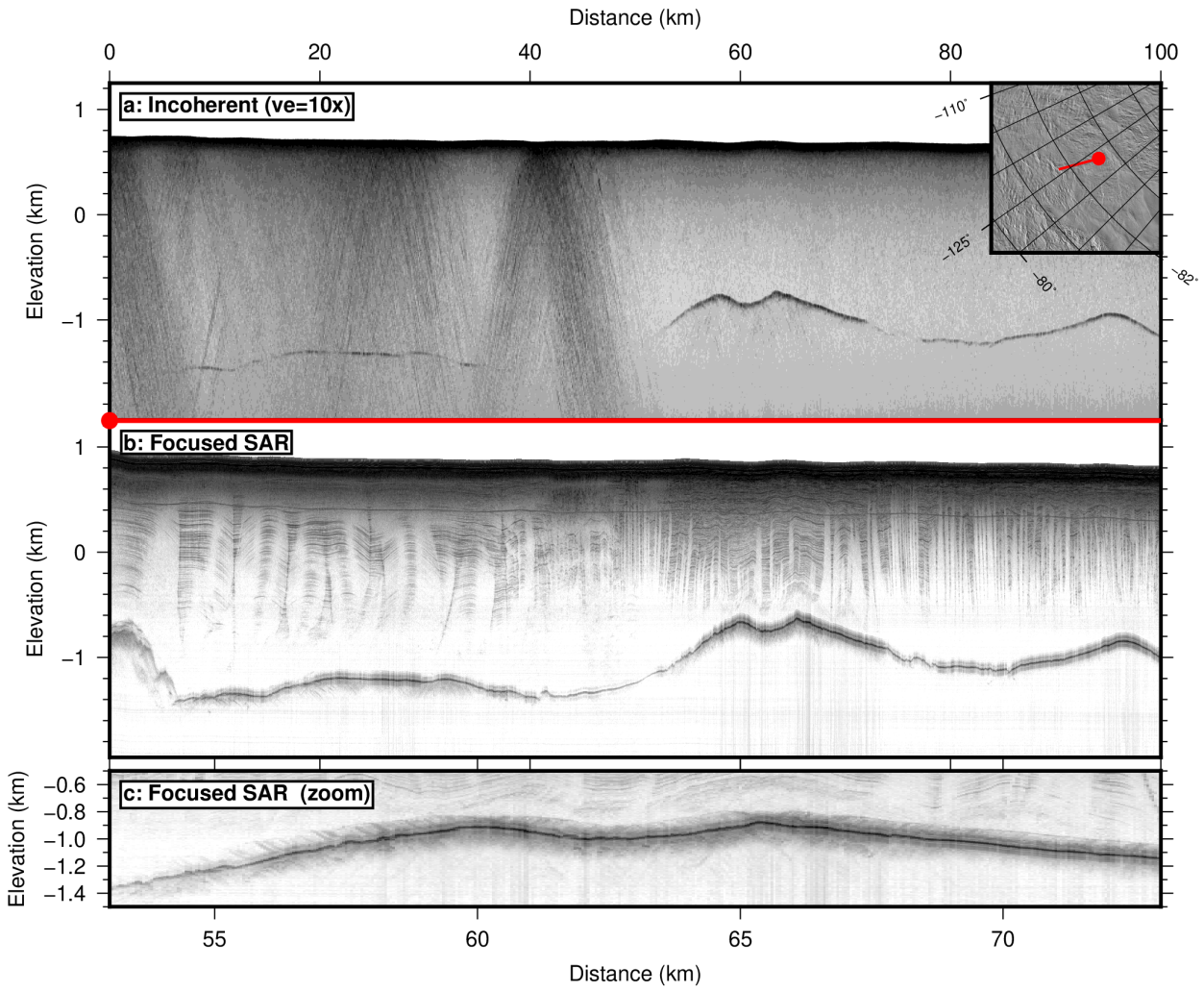

Figure 3: Comparison between types of radar processing and products. a: Depth corrected incoherent radargram from CASERTZ (IRE/WCy/Y09a, flown in 1993, (Blankenship et al., 2001)) over the Kamb Ice Stream volcanic edifice (vertical exaggeration is 10x). b: Depth corrected 2D focused radargram (OND/SJB2/C1D01a) from reflight on same line with HiCARS in 2001 ((Peters et al., 2007) (vertical exaggeration is 10x). c: zoom in on peak of Kamb Ice Stream volcanic edifice, showing englacial reflectors non-conformable with the bed interface. (vertical exaggeration is 2.5x). See Fig. 6 for more discussion.

Geometry of radar interfaces: Radar reflectors constrain the shape of the ice surface, bed topography, and englacial layers, and can provide evidence for the presence of active subglacial volcanoes in a number of ways. The subglacial bed topography can reveal volcanic constructs based on analysis of the morphology and aspect ratio of the topographic relief (*van Wyk de Vries et al., 2018*). The internal structure of the ice sheet, revealed by tracing englacial layers, provides a record of changes in surface accumulation rates, ice flow patterns and basal melt rates in the region. Basal melt rates have been constrained from radar layer draw down (*Fahnestock et al., 2001*). In areas of known or negligible basal friction, excessive basal melt production and layer draw down formations can be indicative of anomalously high subglacial geothermal flux and volcanic activity (Fig. 3 c). Excessive basal melt and internal deformation in the ice column associated with active subglacial volcanism can also create a depression in the ice surface sometimes called ice cauldrons, (*Björnsson, 2003; Gudmundsson, 1996; Gudmundsson &*

Högnadóttir, 2007), which can be detected by IPR and higher precision laser altimeters, and can thus be used to infer areas of active subglacial volcanism (*Blankenship et al., 1993*).

Properties of radar interfaces: The most common properties of interfaces that can be extrapolated from IPR echoes are the reflectivity, roughness, and specularity content. While reflectivity is a measure of the strength of a radar reflector, which is proportional to the contrast in dielectric constants between two adjacent materials, roughness and specularity are a measure of the angular spread of IPR echo return energy. Specularity content refers to the ratio of specular over diffuse radar echo return energy, where specular returns identify mirror-like surfaces that reflect waves along the same incident path, and diffuse surfaces scatter the incident wave across a wider range of angles. Water is highly specular while rock and sediments behave more like diffuse surfaces (*Schroeder et al., 2016*). Specularity content can be thought of as small (wavelength-) scale roughness, or roughness calculated over a shorter evaluation length. One advantage of specularity content is its insensitivity to attenuation of the radar signal through the ice column, which is the biggest source of uncertainty in reflectivity analyses. The joint interpretation of radar interface character can therefore elucidate the properties and structure of the bounding media.

Liquid water has much higher dielectric permittivity compared to rock, sediment, and ice. Therefore water at the ice/bed interface can be detected as a strongly reflective, smooth, and specular reflector relative to the surroundings (*Gudmandsen, 1971; Peters et al., 2005*). While bed echo reflectivity and specularity have been used to detect basal water (*Peters et al., 2005; Schroeder et al., 2014*), anisotropy in specularity observations has been used to characterize subglacial water distribution networks (*Schroeder et al., 2015*).

A combination of IPR subglacial water detection and characterization techniques was used together with a subglacial water routing and glaciological model to assess melt production due to elevated geothermal flux and map active subglacial volcanism in the Thwaites Glacier catchment (*Schroeder et al., 2014*). Similarly, the property of ash layers to produce highly reflective englacial layers through volume scattering has been used to map the extent of a volcanic eruption fall-out in the Hudson Mountains and identify the potential source of a subglacial volcanic eruption (*Corr & Vaughan, 2008*).

Limitations in radar interface interpretation: Accurate interpretation of radar interface geometries relies on three main factors: the survey line spacing, the interpolation algorithm, and the radar acquisition system and processing technique. The spacing between survey lines impacts the final resolution of interpolation products such as Digital Elevation Models (DEM). Line spacing is a function of the survey design, usually optimized for the specific science goals of each survey. Exploratory surveys maximize areal coverage at the expense of resolution, while the opposite is true for targeted surveys. Aerogeophysical surveys can have line spacing between a few to tens of kilometers depending on whether the survey was flown with a helicopter or fixed wing airplane, respectively. Ground surveys can achieve the highest level of detail with line spacing that can vary between hundreds to a few meters but are usually extremely target specific due to the limit in range of this kind of operation.

The type of radar acquisition system utilized and the subsequent type of processing applied to radar data, largely impact the observed geometry of radar interfaces (Fig. 3). The most accurate geometries are rendered by phase-preserving coherent radar acquisition systems (such as HiCARS (*Peters et al., 2005*) and HiCARS2 (*Young et al., 2015*)) combined with focusing techniques that trace the energy of reflectors to their locations or origin in a radar profile

(e.g.(*Peters et al., 2007*); Fig. 3 a and b). This processing removes hyperbolae tails in the radar echoes that would otherwise mask subglacial features such as mountains with slopes similar to or greater than the apparent slopes of the hyperbolae tails. The interpolation algorithm applied to generate DEMs of the bed, surface, and englacial layers elevation are subject to a number of trade-offs including computational costs, mesh grid sizes, accuracy of results and smoothing techniques. In a rough terrain, the resulting bedrock DEMs often represent smoothed estimates for mountain peaks and valley troughs.

Limitations in both data acquisition and processing techniques can therefore fundamentally impair geometries detected by IPR and all interpolated products derived from it, ultimately invalidating interpretations. One example is the subglacial volcano catalog compiled by *van Wyk de Vries et al., (2018),* which is based on direct interpretation of the Bedmap2 bed morphology (*Fretwell et al., 2013*) to identify subglacial shield volcanoes. However, the large data acquisition gaps present at the time of Bedmap2 products release (e.g. in MBL) and the use of a smoothing interpolation spline generated a final bed topography DEM that deviates by hundreds of meters from the input IPR data values with significant induced errors in inferred bed slope (Fig. 4).

Without a systematic analysis of independent data sets supporting the volcanogenic nature of characteristic bedrock peaks (such as potential fields, seismic, and surface elevation data), the aspect ratio of erosional features, especially in sediment rich regions, can easily lead to their misinterpretation as shield volcanos. Fig. 11 shows the locations of the sites proposed by *van Wyk de Vries et al., (2018)* (corrected for a projection error from the coordinates originally reported in Table 2 of that paper). Many of these targets lie either in the interfluvs or the center line of tributaries of the Siple Coast ice streams (Fig. 11) and may instead be erosional features. Finally, Bedmap2 data from most of *van Wyk de Vries et al., (2018)* targets were constrained either by incoherent profiles collected in the 1990s (which will inherently smooth rough landscapes), or SPRI point ice thickness data separated by 2 km (and with poor geolocation (*Bingham & Siegert, 2007*)). This sparsely sampled and smoothed topography will invalidate many of the if not most of the sloped/aspect ratios used to infer "shield volcanoes" by *van Wyk de Vries et al., (2018).*

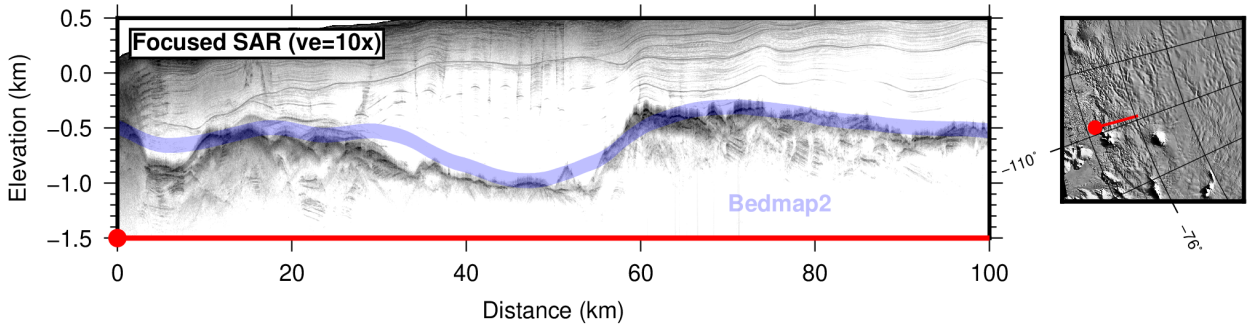

Figure 4: Comparison between bed elevation products along survey line THW/SJB2/X53d. Blue: bed elevation traced from unfocused radar; black: bed elevation traced from focused radar; gray: Bedmap2 bed elevation interpolation showing ±67 m uncertainty, as determined for Carson Inlet, West Antarctica (Fretwell et al., 2013).

The interpretation of layer draw down geometry relies on the existence, persistence, and continuity of layers in radar measurements. It is important to note that the interpretation of

layer draw downs are non-unique. A number of processes unrelated to volcanic activity can similarly deform the ice column and englacial layers (*Siegert et al., 2004*). Mechanical deformation due to ice flow over a subglacial obstacle, variations in vertical strain rates (*Raymond, 1983*), ice sheet surface slope variations due to changes in surface accumulation rates (*Vaughan et al., 1999*), and changes in ice flow direction (*Siegert et al., 2004*) deform layers in similar ways. Here we refer to anomalous layer draw downs as layer geometries which cannot be explained by geo- or ice-dynamic processes other than melting from elevated geothermal heat. Similarly, the presence of water at the ice-rock interface is non-unique to geothermal heating nor is it indicative of processes that take place in-situ, at the location where water is detected. Water can be produced locally by basal frictional heating or advected from higher hydropotential regions and shall therefore be representative of processes characteristic of different glaciological/geological settings.

Furthermore, the strength of bed echoes, and thus the interpretation of the presence of subglacial water, is affected by a combination of englacial attenuation (*Matsuoka, 2011*) and the material and geometric properties of the ice sheet and bed, which can introduce ambiguities in quantitative echo interpretations.

Potential fields

As gravity and magnetic field data smooth as a function of distance from the source, volcanic anomalies related to processes at the ice-rock interface should have relatively high frequency content compared to deep crustal processes. Limitations to detection of volcanic constructs from potential fields data often arise from the original data acquisition parameters. Both line spacing and source to sensor distance impose limits on the smallest resolvable feature size and require surveys to be designed accordingly.

Gravity: The gravity field can be measured from an aircraft by stable measurement of vertical accelerations, and then subtraction of the acceleration due to the motion of the aircraft. Subtraction of the global reference gravity field predicted at the aircraft's location, and compensation for the Earth' rotation, provides gravity disturbances which are due to deviations in the total mass under the aircraft from a homogeneous model. The spatial variability of the remaining heterogenous gravity field can provide information on the depth of sources. In Antarctica, the dominant source of gravity disturbances is the ice-rock interface, with the second strongest source being the density contrast between the crust and the mantle. With knowledge of the ice-rock interface, the two sources can be untangled by calculating the Bouguer anomaly. The crustal structure and other spatial density contrasts can be inferred from gravity disturbances and are commonly used to determine crustal thickness and sediment distribution (e. g. *Damiani et al., (2014)*).

The fundamental limit on the resolution of gravity measurements is proportional to the distance between the sensor and the source; given the thickness of ice in Antarctica, this means that gravity is less of a tool for directly inferring the density of volcanic deposits, and more useful for determining the geological context for these features. However, large mafic intrusive bodies within a sedimentary crust may have a significant positive gravity anomaly.

Magnetics: The character and pattern of magnetic anomalies are used to map the distribution of igneous rocks, which have high content in magnetic minerals and high magnetic susceptibility. Magnetic anomalies can be modeled with both forward and inverse methods to define the shape and depth of the source igneous body (*Turcotte & Schubert, 2014*). High magnetic susceptibility

values required to simulate observed magnetic anomalies, especially when closely associated with subglacial topographic features observed in radar data, are evidence for bedrock of volcanic origin. Similarly, particular spatial patterns of magnetic anomalies are often good indicators for volcanic origin and activity. As such, circular, "donut shaped" patterns of high amplitude magnetic anomalies surrounding central magnetic lows mark known volcanically active or young calderas, such as in Yellowstone and the Rocky Mountains area of the US (*Bhattacharyya & Leu, (1975); Smith & Braile, (1994)*, see Fig. 5 b).

The magnetization of rocks is a function not only of the presence of magnetic minerals, but also temperature. Intrusive and extrusive igneous bodies only consist of a magnetic anomaly if the rocks have cooled below the Curie temperature of magnetite (580 °C), whereas hot, molten igneous rock at or above the Curie temperature show no magnetic signature. This leads to the characteristic magnetic "donut" shape anomaly seen in active volcanic centers, showing a negligible (close to zero) low amplitude magnetic signal surrounded by high amplitude magnetic anomalies.

The 100,000 year limit we impose on the search for active subglacial volcanism helps us narrow the search for positive magnetic anomalies. Since the last major magnetic reversal was 780,000 years ago (*Singer, 2014*), negative anomalies, if due to negative remnant anomaly, should be older than 1 Ma and therefore outside our interval of interest. A brief complete reversal, the Laschamp excursion, occurred only 41,000 years ago during the last glacial (*Singer et al., 2009*). That reversal though lasted only about 440 years and the actual change of polarity lasted around 250 years.

Joint inversions of magnetic and gravity anomalies are used to test if sources are shared (i. e. a cold, magnetized mafic intrusive) or separated (a hot demagnetized dense body with shallow or offset magnetic sources) and thus test hypotheses for the activity of candidate sites (see section on Kamb Ice Stream).

Seismology

Deep long-period (DLP) earthquakes are a type of volcano-seismic activity identified in many volcanic settings including the Aleutian Islands, the Pacific Northwest of North America, Hawaii, and Mount Pinatubo (*Nichols et al., 2011; Okubo & Wolfe, 2008; Power et al., 2004*). DLP are characterized by deep hypocenters (at or below the brittle–ductile transition zone), low-frequency energy (< 5 Hz), and swarm behavior (*Okubo & Wolfe, 2008*) and are hypothesized to represent the movement of magma and other fluids within volcanic and hydrothermal systems.

Seismic data also reveals variability in seismic wave velocity and patterns of mantle anisotropy, which are used to image the distribution of thermal anomalies within the mantle and estimate crustal thickness. In West Antarctica, 10 permanent co-located GPS and broadband seismic stations measure relative plate motion and seismicity in central WARS as part of the Antarctic Polar Earth Observing Network (ANET-POLENET). To improve spatial coverage and produce higher-resolution tomography, during the 2010-2012 POLENET campaign an additional 13 temporary stations were installed across the WARS between the Whitmore Mountains and Marie Byrd Land (*Emry et al., 2015; Hansen et al., 2014; Heeszel et al., 2016; Lloyd et al., 2015*).

Direct measurements

Direct measurements of geothermal flux via borehole thermometry are extremely difficult to undertake due to inaccessibility of the ice sheet bed. Ice borehole data coverage is also limited and therefore not representative of large regions. In addition, this type of measurement only provides a minimum bound on geothermal flux since basal melting, if present, would reduce heat conduction into the overlying flowing ice (*Engelhardt, 2004b*). Over the last decade, borehole measurements of heat flow have expanded with the WAIS Divide ice core site, and measurements through direct access to the bedrock in the Siple Coast (*Begeman et al., 2017*). The results indicate considerable variability in geothermal heat flux that is consistent with active volcanism (*Fisher et al., 2015*).

In addition, ice cores can sample englacial ash deposits (*Iverson et al., 2017; McConnell et al., 2017; Palais et al., 1988*) providing a datable indicator for potential subglacial eruptions. Direct measurements thus provide valuable point constraints for geophysical methods.

Active subglacial volcanic sectors

We group active subglacial volcano candidates into sectors based on the portion of WAIS that is impacted by their activity (Table 1; Fig. 11). Available datasets are evaluated for evidence of active volcanism at each candidate site.

Table 1. Characteristics of volcanic sectors. These sectors include deep and shallow bed rock, fast and slow flow, and variations in overall crustal thickness. Driving stress is a parameter calculated from ice surface slope and ice thickness that indicates the degree of coupling of ice to its bed and shear margins.

Sector	Ice flow organization (Mouginot et al., 2019)	Driving stress (Sergienko et al., 2014)	Bed elevation (Ice Thickness) (Fretwell et al., 2013)	Crustal thickness (Chaput et al., 2014)
Siple Coast	Fast ice streams	Low	~ -0.5 km (~ 1km)	~ 30 km
WAIS divide	Low to no flow	Low to none	~ -0.5 to -1.5 km (~2.5 to 4 km)	< 25 km
Marie Byrd Land	Low flow	Low	~0.5 to -0.5 km (~ 1 to 2 km)	~ 30 km
Amundsen	Fast ice streams	High	~ -1.5 km (~ 2 to 3 km)	~ 25 km

Siple Coast sector

The Siple Coast is located within a low relief region of the WARS characterized by relatively thin crust (Chaput et al., 2014). It is bounded by the EWM crustal block and the Transantarctic Mountains to the South and by wMBL to the North.

Subglacial volcanic activity in this region is of particular interest since subglacial melt water production sustained by elevated geothermal flux has the potential to impact ice stream dynamics along the Siple Coast. The Siple Coast's ice streams are characterized by low driving

stress due to low ice surface slopes and lack of strong topographic bed control, which makes the presence of basal water essential to sustaining ice flow through basal sliding. Moreover, the low driving stresses of the Siple Coast allow thinning of the ice streams and reduced basal shearing, both of which act to cool the bed and promote basal freezing (Christoffersen et al., 2014). Fluctuations in water supply can therefore cause the thin ice streams to stagnate through rapid freeze-on at their bases. To mobilize ice streams with such thin ice in low shear stress configurations, a large supply of subglacial water from the interior is required.

Mt. CASERTZ edifice

Subglacial volcanic activity at Mt. CASERTZ was first identified by *Blankenship et al., (1993)* from radar, laser and magnetic data evidence (Fig. 5) and later supported by analysis of englacial ash layers compatible with subglacial eruptions sourced at Mt. CASERTZ (*Iverson et al., 2017*). Mt. CASERTZ is located northwest of the Whitmore Mountains, in the transition zone between the EWM crustal block and the Ross Subglacial Basin, along an ice tributary ~ 100-200 km upslope of the Siple Coast's area of ice stream initiation (*Blankenship et al., (2001)*, Fig. 1d)

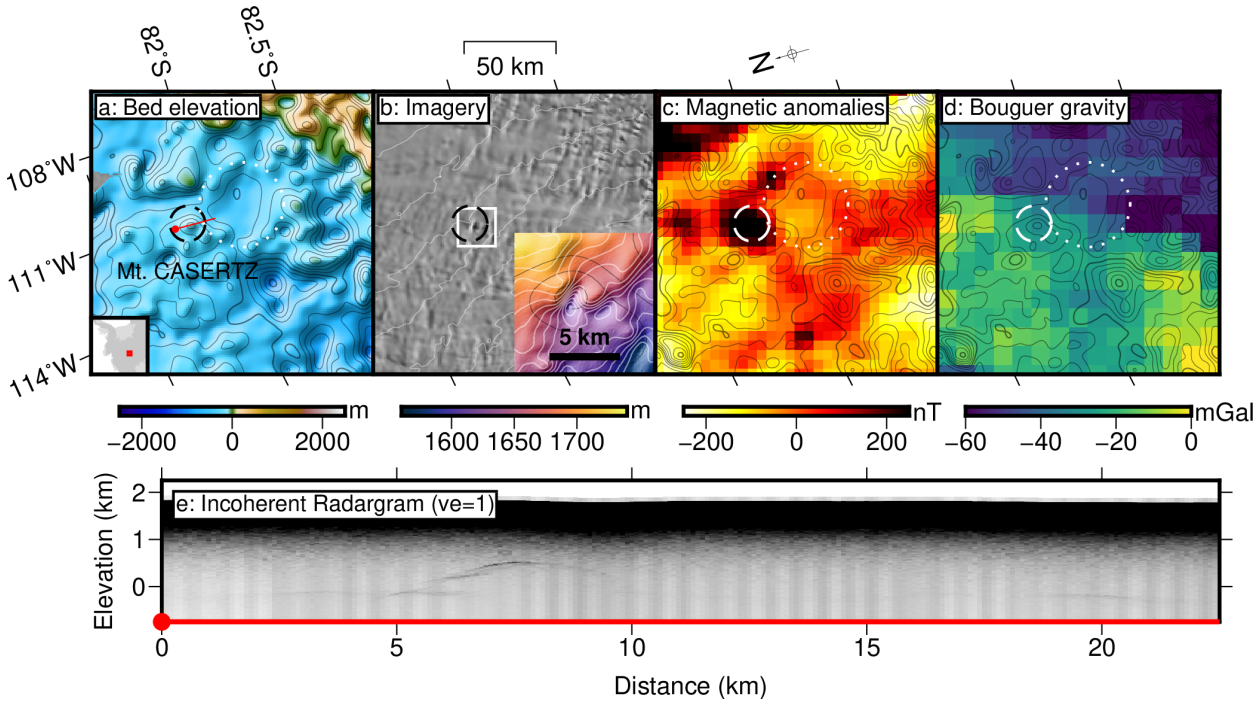

Figure 5: Observations of Mt. CASERTZ (from (Blankenship et al., 1993)). a) Bedrock topography: red line is part of profile shown in Fig. 5 e, ball is start of line. Mt. CASERTZ is dashed circular, associated caldera is dotted circle. 100 m bedrock elevation contours are in black for all. b) Imagery from MOA (Scambos et al., 2007). White box shows insert. Insert shows ice surface topography from the Reference Elevation Map of Antarctica (REMA, (Howat et al., 2019)). 10 m surface contours in white. c) Magnetic anomalies from ADMAP2 (Golynsky et al., 2018). d) Bouguer gravity anomaly from (Scheinert et al., 2016). e) Depth corrected incoherent radargram from 1991-92 CASERTZ field campaign, part of transect IRE/NEy/Y05a, with no vertical exaggeration. Edifice is at 7 km along track). This transect was flown relatively high at 1000 m above the surface for stable gravity, allowing for significant surface scattering (black band at top), obscuring englacial layers.

Mt. CASERTZ shows as a cone-shaped subglacial topographic edifice about 6 km across that rises ~ 650 m above the surroundings (Fig. 5 a, *Blankenship et al., (1993)*). Mt. CASERTZ stands on the edge of a ~ 50 km-wide caldera bounded by a rim 100-200 m in height. The cone's steep slopes (~ 12°, Figure 5 e) indicate that the edifice was extruded into the ice or possibly under shallow water before the development of the WAIS. The ice surface elevation at the location of Mt. CASERTZ's central edifice shows a 48 m deep depression (Fig. 5 b). Following the regional ice flow pattern, ice from further upstream enters the surface depression from the north and south, indicating that the large ice surface anomaly requires a 10-20 W/m^2 heat source at the base (over two orders of magnitude more than the continental average geothermal flux), melting ~ 0.07 km^3 of ice each year, to be sustained.

A large-amplitude (~ 600 nT), long-wavelength, positive magnetic anomaly ~ 40-80 km in diameter suggests that both the caldera and central edifice are part of a larger volcanic construct (*Blankenship et al., (1993)*, Fig. 5 c). The large magnetic anomaly is associated with a broad uplift of the bedrock topography. The modeled underlying intrusive appears to be several kilometers thick, assuming the material producing the magnetic anomaly has a magnetic susceptibility 0.10 SI (*Behrendt et al., 1995*). The complex is located on a boundary in crustal thickness, as implied by gradients in Bouguer anomalies (*Blankenship et al., (2001)*, Fig. 5 d).

The bed radar echo strength at the location of Mt. CASERTZ is weaker compared to those in areas of both equivalent and larger ice thickness in West Antarctica. The bed echo strength is sensitive to the temperature - dependent dielectric attenuation of radio waves through ice, indicating the ice above the central edifice is anomalously warm (*Blankenship et al., 1993*).

The bed radar echoes show tails of diffraction hyperbolae characteristic of rugged terrains (Fig. 5 e, *Blankenship et al., (1993)*). The composition of the central edifice is therefore consistent with a pile of pillow lavas and hyaloclastite material. Unlike a coherent shield, this pile of scatterers is likely poorly consolidated material that would be easily eroded by ice (*Behrendt et al., (1995)*, Fig. 2), indicating that Mt. CASERTZ is a recently erupted volcano that has not yet suffered removal by the overlying ice sheet (*Blankenship et al., 1993*).

Kamb Ice Stream subglacial edifice

The joint interpretation of potential fields and radar sounding data collected by the University of Texas Institute for Geophysics (UTIG) indicate a subglacial active volcano candidate in the onset region of the Kamb Ice Stream (KIS) of West Antarctica, few tens of km north of the transition zone between the EWM microplate and Ross Subglacial Basin. The lower parts of KIS are known to have been stagnant for the last ~150 years (*Retzlaff & Bentley, 1993*), while upstream ice continues to flow (*Price et al., 2001*).

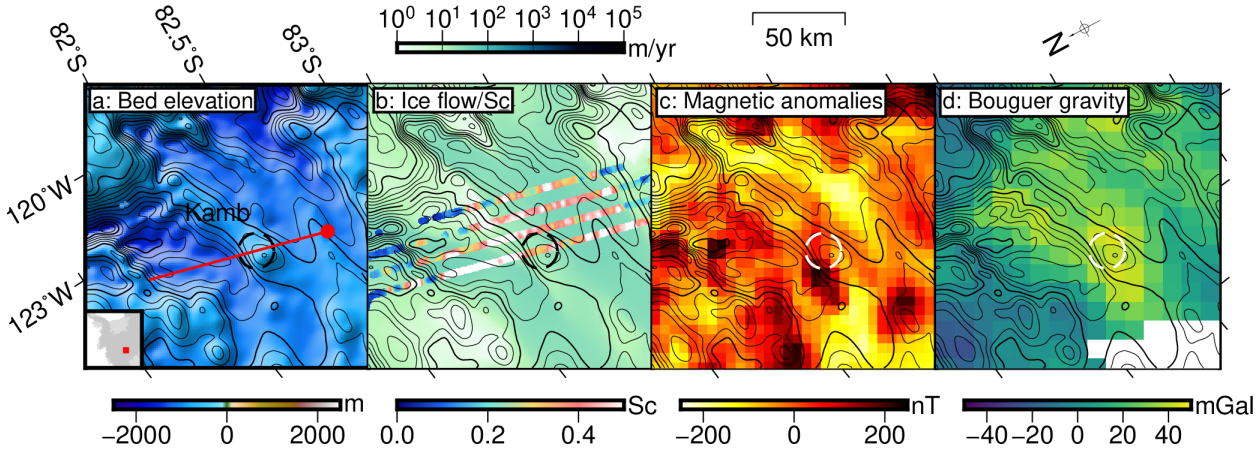

Figure 6: Volcanic feature at the head of the stalled Kamb Ice Stream. Polar Stereographic projected km used as coordinates, bed topography contours in 100 m intervals shown on all. a: Bedrock topography; red line is the line of section shown in Fig. 3, ball indicates start of line. b: Specularity content (S_c, (Young et al., 2015)) superposed on surface ice flow velocity (Mouginot et al., 2019). High S_c indicates subglacial water. c: ADMAP-2 magnetic anomalies (Golynsky et al., 2018). d: Bouguer gravity anomalies (Scheinert et al., 2016). High values are consistent with either a dense body in the crust or an upwarp of the crust/mantle interface.

The KIS subglacial volcano was first surveyed in 1992 during the CASERTZ aerogeophysical survey with incoherent radar (*Blankenship et al., (2001)* Fig. 3 a) before being partially reflown with HiCARS as part of the ATRS program (*Peters et al., 2007, 2005*). HiCARS focused data shows englacial layers that dip into the edge of a broad conical high in the center of the ice stream (Fig. 3 c). Radar sounding over the KIS onset region shows a bright sub-ice reflection (*Peters et al., 2007*) and high specularity content suggesting the presence of significant water beneath the ice stream (Fig. 6 b, *Young et al., (2015)*).

Joint interpretation of the high gravity signal and relatively weak magnetic signature suggests the presence of a subglacial volcano in the area. Magnetic anomalies are relativily weak, narrow and offset from topography (Fig. 6 c). This volcanic feature, however, produces a sharp distinctive peak in Bouguer gravity (Fig. 6 d) centered on the edifice, likely due to a high density contrast between a magma body in the subsurface and the surrounding rocks, but a low magnetic signature due to a thin layer of extrusive material just beneath the ice. A single body does not satisfy the gravity, magnetic and topographic constraints, suggesting a deep high density body too hot to have a magnetic signature, and a carapace of thin cool magnetic material surrounding the edifice with the dipping englacial reflectors.

Subglacial Lake Whillans heatflow anomaly

Extraordinary high geothermal flux (285 ± 80 mW m^{-2}) was measured at Subglacial Lake Whillans (SLW) drilling site as part of the Whillans Ice Stream Subglacial Access Research Drilling (WISSARD) project (*Fisher et al., 2015*). The measurement represents the first direct assessment of geothermal flux into the base of WAIS, obtained with a probe that went ~ 1 m deep into basal sediments. The value of geothermal flux determined at SLW is significantly higher than continental average but representative of areas of active hydrothermal and volcanic activity (e.g. http://www.heatflow.org). A second WISSARD probe 100 km away near the grounding line of Whillians Ice Shelf found a heat flux of 88 ± 7 mW m^{-2} (*Begeman et al., 2017*),

while an ice borehole at Siple Dome, where the bed is inferred to be frozen to the bed, yielded a geothermal heat flux of 70 mW m^{-2} (*Engelhardt, 2004a*), both consistent with rifted continental crust (*Davies, 2013*).

The highly dynamic hydrologic activity observed at the SLW drilling site (*Fricker & Padman, 2012*) is consistent with fluctuations of basal melt water supply generated by elevated geothermal flux. The site location near the convergence between Siple Coast's Whillans and Mercer Ice Streams makes changes in the local hydrologic configuration particularly relevant to ice sheet dynamics.

No edifice is observed at Subglacial Lake Whillans (*Christianson et al., 2012*), instead a minor bedrock depression, consistent with the high ice velocity in this area (Fig. 1 d).

WAIS divide sector

The WAIS divide sector is located within the low lying cradle-shaped topography of the central WARS, up to 2000 m below sea level, characterized by thin crust (*Chaput et al., 2014; Fretwell et al., 2013*). It is bounded by the EWM crustal block to the south and the eastern MBL crustal block to the north. The WAIS divide is a region of thick ice and slow to negligible ice flow (Fig. 1 c,d). Similar to a continental hydrographic divide, this region separates the WAIS into two catchments: one where the ice flows to the Ross Sea, and one where the ice flows to the Amundsen and Weddell Seas. Subglacial volcanic activity in this sector can impact ice organization within those catchments, which can ultimately lead to ice divide migration.

Detailed shard morphology characterization and geochemical and micro-CT analyses of two tephra layers from the WAIS divide ice core suggest a phreatomagmatic origin from a subglacial or close to emergent volcano (*Iverson et al., 2017*). The tephra layers were erupted from the center of the WAIS, making Mt. CASERTZ one of the potential subglacial volcanoes that sourced the layers.

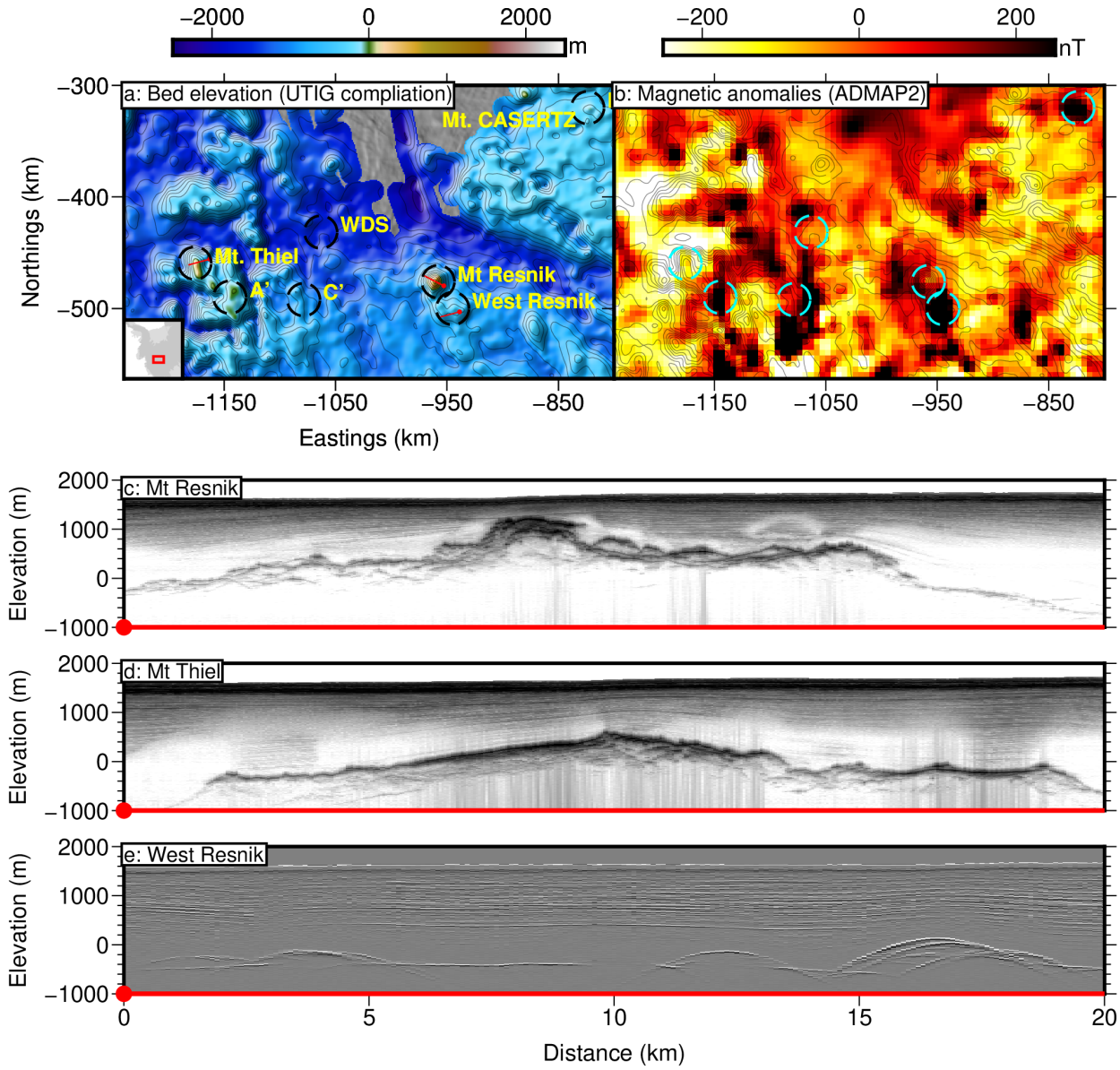

Figure 7: Map of the central region of the WAIS divide sector, showing a) bed elevation and the locations of the volcanic features discussed in this section b) ADMAP-2 magnetic anomalies (Golynsky et al., 2018)) and radargrams with 1.5x vertical exaggeration of c) Mt. Resnik (transect OND/SJB2/DVD01a, focused), d) Mt. Thiel (transect THW/SJB2/Y51a, focused) and e) a low lying region west of Mt Resnik (transect BSB/Wy/Y19a, incoherent).

WAIS ice core site heatflow anomaly

The high precision measurements made in the 3405-m deep borehole at the WAIS Divide ice core site (WDS, *Fudge et al., 2013*) (Fig. 7), represent the first direct measurement of anomalously high subglacial geothermal flux in Antarctica, calculated from vertical strain rates in the ice to 50 m above the estimated bedrock depth, where drilling stopped to prevent contamination of the basal hydrology. Site selection for the WAIS Divide ice core had been part of an effort by the ice coring community to find an ice record extending to the last interglacial in West Antarctica.

Criteria for site selection included finding a region with thick ice and slow ice flow, to assure recovery of deep/old and undisturbed/organized ice record (*Morse et al., 2002*).

However, despite the great ice thickness (> 3000 m) and the slow ice flow at WDS, the ice near the bed proved to be relatively young (~ 68 ka) compared to shallower cores drilled in central East Antarctica, which was interpreted as the result of high accumulation rates (22 cm a^{-1} at present and ~ 10 cm a^{-1} during the Last Glacial Maximum) and basal melt (*Buizert et al., 2015*).

Interpretation of the temperature measurements in the borehole indicates the ice sheet is melted at the bed at this location and that the basal melting rate is remarkably high, ~ 1.5 cm a^{-1}. The inferred geothermal heat flux, using thermal data from the ice sheet and a one-dimensional model of ice dynamics, is estimated to be about 140 to 220 mW m^{-2}, 4–5 times the continental average. Importantly, the absence of a surface depression at WDS indicates that this high heat flow is likely to be the regional value (horizontal scale ~ 30 km), rather than simply a local anomaly. IPR data indicates a very flat ice-bed interface, with no significant local volcanic edifices. WDS is located in a gap between two significant magnetic anomalies (Fig. 7), which is consistent with thermal suppression of magnetic susceptibility.

Central WAIS caldera complex

A series of positive magnetic anomalies between 400 and 1200 nT surrounding a central magnetic low (~ -150 nT) define the rim of what has been inferred to be a large subglacial caldera about 70 km in diameter located in the deep ice region between MBL and the WAIS Divide ice core site (Figs. 1, 7; *Behrendt et al., (1998*)). The caldera is surrounded by a low magnetic background (-300 to -500 nT), consistent with a shallow Curie isotherm (*Behrendt et al., 1998*). The magnetically defined caldera lies on the "sinuous ridge" subglacial range under the Thwaites Glacier/Siple Coast Divide that was first defined by sparse radar sounding data by *Jankowski & Drewry, (1981).* Additional soundings reveal that this range is highly dissected by deep subglacial valleys (*Behrendt et al., 1998; Holt et al., 2006*).

Behrendt et al., (1998) inferred from an early analysis of the IPR data that these magnetic anomalies were largely decorrelated from bedrock topography, with the exception of one magnetic anomaly on the the southwest rim (called "C" by *Behrendt et al., (1998),* see Fig 3 from that paper), where current ice thickness is about 3 km. *Behrendt et al.'s (1998)* observation suggested that the source rock for anomaly C may consist of erosion resistant pillow lavas, characteristic of eruptions under very thick ice and supports the interpretation that the caldera complex was recently active under the current, thick WAIS.

However, reexamining the magnetics and radar data, it appears that the original interpretation had a 30 km along track offset (see Fig. 8 for an updated coregistration). Magnetic anomaly C no longer aligns with a deep bedrock peak (C') but is offset. C' is surrounded by bright bed returns and overlaid by disturbed englacial layers while a second, weaker magnetic anomaly (called A by *Behrendt et al., (1998))* aligns closely with a shallower bedrock peak (A'). We suggest that the subglacial mountain C', offset from anomaly C, may still be warm (and thus have a locally suppressed magnetic anomaly), while A' may represent an old subaerial volcano composed of solidified lava, which after rebound may have risen above sea level, that is preserved by its proximity to the ice divide.

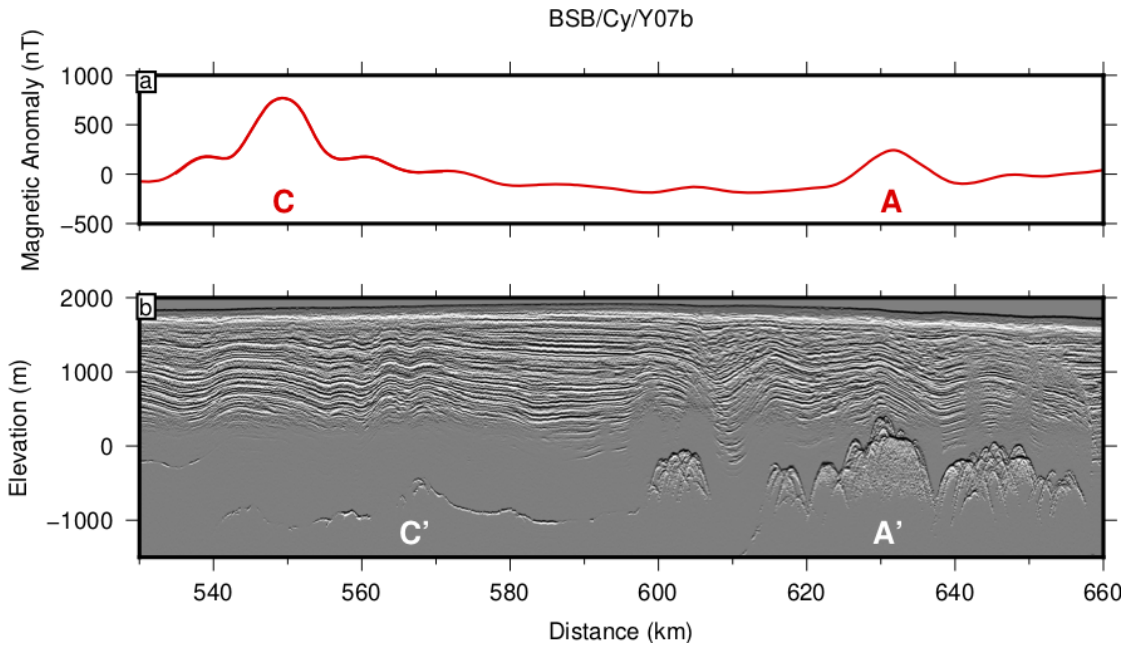

Figure 8: Updated CASERTZ profile (BSB/Cy/Y07b) across the proposed subglacial caldera complex under the Thwaites/Siple Coast ice divide. Compare with Fig. 3 of (Behrendt et al., 1998). a) magnetic anomaly from (Sweeney et al., 1999). b) depth-corrected incoherent radargram, differentiated for clarity. 10x vertical exaggeration. Note that these radar data are unfocused.

Mt Resnik edifice

Mt Resnik (informally named after late astronaut Judith Resnik) is a major subglacial edifice near the Bentley Subglacial Trench (Fig 7 a), which has a negative magnetic anomaly (*Behrendt et al., (2006),* Fig 7 b). It is unlikely that Mt. Resnik was entirely built in 250 yrs of the Laschamp event, therefore the negative magnetic anomaly of Mt. Resnik dates this volcano at more than 0.8 Ma therefore too old and too cold to have had an impact on the current ice sheet. *Iverson et al., (2017)* concluded that Mt Resnik was the most likely source for the subglacial ash layer in the WAIS Divide ice core, based on its shallow depth of burial (~ 300 m). However, the significant amount of erosion apparent on the upper part of the edifice in focused radar data (Fig. 7 c) when compared to other edifices under the WAIS also imply that Mt. Resnik is not significantly active today. An alternative geomorphic interpretation of Mt. Resnik is that it is a 'tuya' or table mountain, formed by a subglacial eruption breaching the surface of the ice; however additional focused radargrams from additional orientations would be required to make a conclusive identification. Mt. Resnik's shallow burial and location in the heart of the main trough of the the WARS makes it an ideal target for reconstructing the collapse history of the WAIS through exposure dating methods (*Spector et al., 2018*).

A site to the west of Mt Resnik does have both a significant magnetic anomaly (Fig. 7 b) and a large number of subglacial peaks (Fig. 7 e); however focused data for assessing the morphology of these features is not yet available.

Mt. Thiel edifice

Mt. Thiel (informally named after late University of Wisconsin geologist Edward Thiel) was first identified from airborne magnetics and interpreted as composed of erosion-resistant lavas by

Behrendt et al., (2002). It has a subglacial topographic relief ~ 1800 m high (Fig. 7 d) and corresponds to a positive (400 nT) magnetic anomaly situated within the low magnetic background and shallow Curie isotherm surrounding the nearby subglacial caldera complex. Unlike Mt. Resnik, the shield of Mt. Thiel is largely intact (Fig. 7 d). Mt. Thiel is located about 100 km distant from the WAIS ice core drilling site and is a hypothesized source of the prominent volcanic ash layer detected at the WAIS Divide ice core (*Behrendt, 2013; Iverson et al., 2017*). The high bed reflectivity of Mt. Thiel, combined with the lack of a catchment for subglacial hydrology, imply heat flows of above 150 mW m^2 (*Schroeder et al., (2014)* at this site, Fig. 1 c,d). Given the intact topography, the proximity to WAIS Divide, and the inference from *Schroeder et al., (2014)*, we classify this volcano as likely active.

Central WAIS fissure system

Magnetic anomalies L and M identified by *Behrendt et al., (1995)* have been analyzed by *Danque (2008)* using focused HiCARS radar and magnetics from the AGASEA survey. *Danque (2008)* inferred the edifice associated with magnetic anomaly M (hereto referred to as M') is both older and colder than the edifice associated with magnetic anomaly L (hereto referred to as L') based on the smooth subglacial topography of edifice M', which is consistent with prolonged erosion and sediment drape (*Behrendt et al., 1995*) and the lack of subglacial lakes (discussed below) uniquely associated with edifice L'. In addition, *Danque (2008)* interpreted an additional anomaly, fissure H, which corresponds to a significant down draw of englacial layers (Fig. 9 d).

In radargrams (eg Fig. 9 d), edifice L' shows as a broad, dome-shaped subglacial edifice about 250-300 meters high with a stair-step morphology and steep ridges on its summit. Coherent radar sounding data over edifice L' show eight bright basal reflections (200-500 m in diameter) located along the breaks in the slope between the surrounding plains and the dome of edifice L'. These bright spots appear in radar profiles as smooth, bright, and specular reflectors located in hydraulic flat regions on the flanks and on the summit of edifice L' and are interpreted as subglacial lakes. Two of the potential lakes found on the summit of edifice L' are located respectively in a depression on the south-east side of the summit and between the summit ridges. The steep-sided ridges on edifice L' could either indicate recent eruption products or an old ridge that is well preserved by the slow flowing ice near the divide.

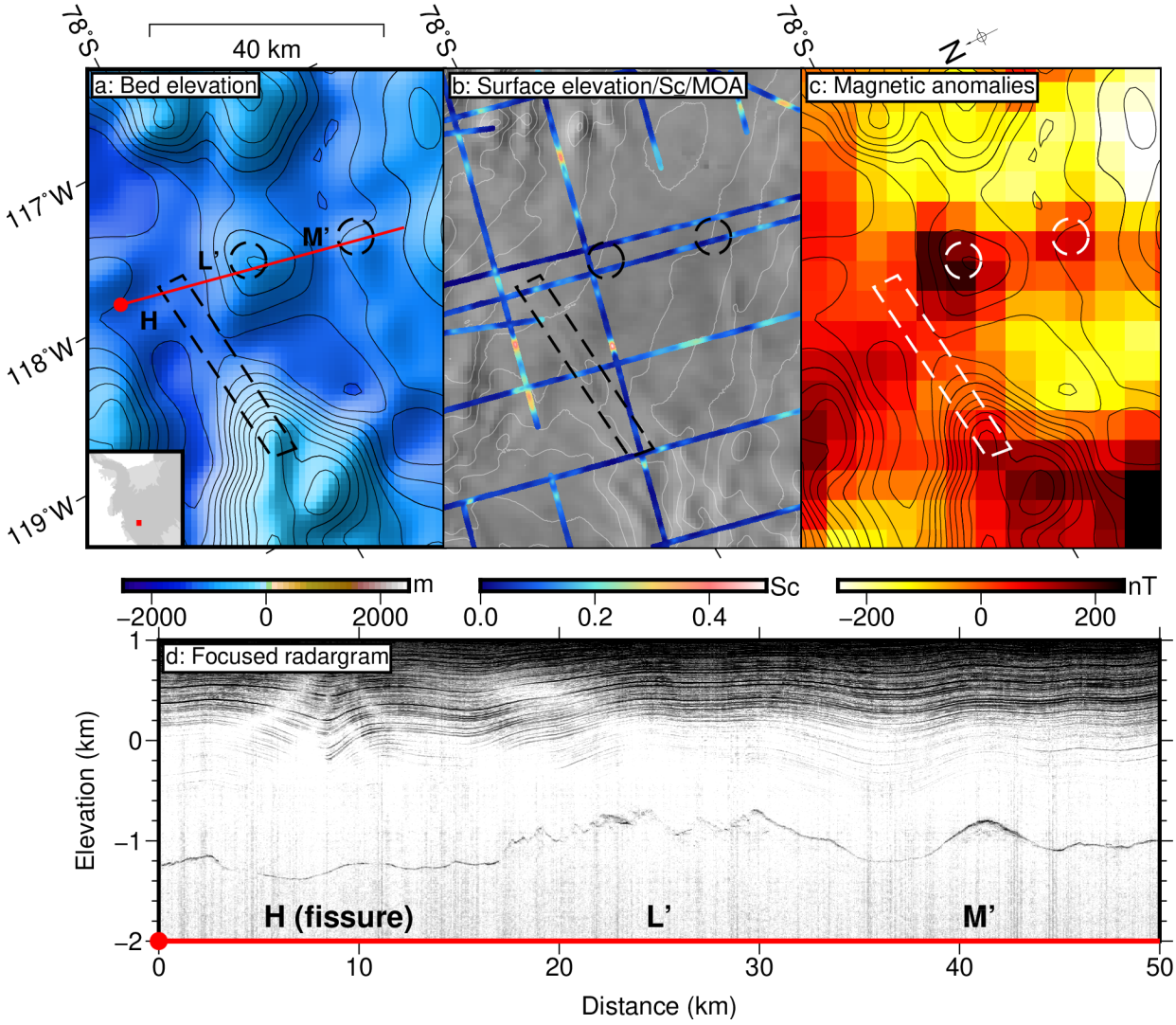

Figure 9: Map of the Fissure region (dashed rectangle) of the WAIS divide, showing a) bed elevation, the locations of the volcanic features and the location of the segment of profile d (red line). b) specularity content (Schroeder et al., 2013; Young et al., 2015) shown on the MOA image mosaic (Scambos et al., 2007) and 10 meter contour lines from the Reference Elevation Map of Antarctica (REMA, white, (Howat et al., 2019)). A faint dark streak is visible in the dashed rectangle in the MOA imagery and affects REMA contours; c) ADMAP-2 magnetic anomalies with bed elevation contours (Golynsky et al., 2018). d) radargram THW/SJB2/X31c showing layer down draw over H. (vertical exaggeration=5x)

Even though the ice surface does not dip over edifice L', the englacial layers have some drawdown over one of these possible lakes, while over the summit of L layers fade out entirely. This might indicate a physical or thermal disturbance over the summit of edifice L' that leads to steep layer slopes dipping > 10 degrees, which is the imaging capabilities of the current 2D-focused Synthetic Aperture Radar (SAR) processing.

A magnetic anomaly ~ 300 nT in amplitude is associated with edifice L'. (Fig. 9 c). The model of the magnetic anomaly is consistent with a large cooling intrusive body hot enough to maintain the subglacial lakes apparent in coherent radar profiles. Because of the position of the lakes with

respect to the regional hydraulic potential, it is likely that the lakes are sustained by local sources and not by subglacial water flow.

Edifice M' (*Behrendt et al., 1995; Danque, 2008*) appears in radargrams as a mound situated along an elongated subglacial ridge oriented nearly east-west, adjacent to edifice L'. Edifice M' is associated with a ~ 300 nT magnetic anomaly, has no corresponding ice surface depression or internal layer drawdowns, and lacks evidence for nearby subglacial lakes (Fig. 9). The low topography and smooth sides are consistent with the interpretation that edifice M' is the eroded root of a subglacial volcanic edifice (*Behrendt et al., 1995*), likely older and colder than edifice L'.

The H fissure (*Danque, 2008*) is a large layer drawdown anomaly in the radar englacial layers of the ice sheet located along an area of flat topography adjacent to edifice L. The layer drawdown is identified by a ~ 300 m dip in the deepest visible englacial layers that can be traced for 28 km in length. A small, ~ 70 m high and ~ 2 km across topographic relief underlies the layer drawdown for the entire length of the anomaly. Bright, flat, and specular echoes on either side of the bed topography relief indicate subglacial lakes 0.5 km and 1 km in apparent cross-sectional diameter. The layer drawdown is associated with an ice surface depression visible in the MOA surface imagery (Fig. 9 b) and a < 50 nT magnetic anomaly (Fig. 9 c). The presence of a positive but relatively suppressed magnetic signal, basal water, and an ice surface depression in a region of negligible ice flow makes this a likely active volcanic site.

Marie Byrd Land sector

The Marie Byrd Land sector is a region of high bed topography and thicker crust (Chaput et al., 2014; Fretwell et al., 2013; LeMasurier, 2006). It is composed of the wMBL and eMBL crustal blocks and bounded to the south by the low lying WARS. It is located hydrologically upstream of the Siple Coast and Amundsen sectors, characterized by fast-flowing ice streams and complex dynamics greatly impacted by changes in subglacial water discharge, which makes volcanism and high geothermal flux in this sector of great importance as a melt water source. Seismic tomography from the broadband seismic POLENET shows evidence for a broad thermal anomaly extending deep into the mantle under Marie Byrd Land (*Hansen et al., 2014*) consistent with a mantle hot spot centered beneath the Executive Committee Range (*Accardo et al., 2014; An et al., 2015; Emry et al., 2015; Heeszel et al., 2016; Lloyd et al., 2015*).

Executive Committee Range edifice

Underground magmatic activity has been identified at the southern tip of the Executive Committee Range volcanic chain from passive seismic observations as part of the POLENET project (*Lough et al., 2013*). A cluster of deep long-period seismic episodes was detected in January-February 2010 and March 2011 beneath a subglacial edifice (Fig. 10) located where present volcanic activity would be expected along the Executive Committee Range volcanic trend north to south migration.

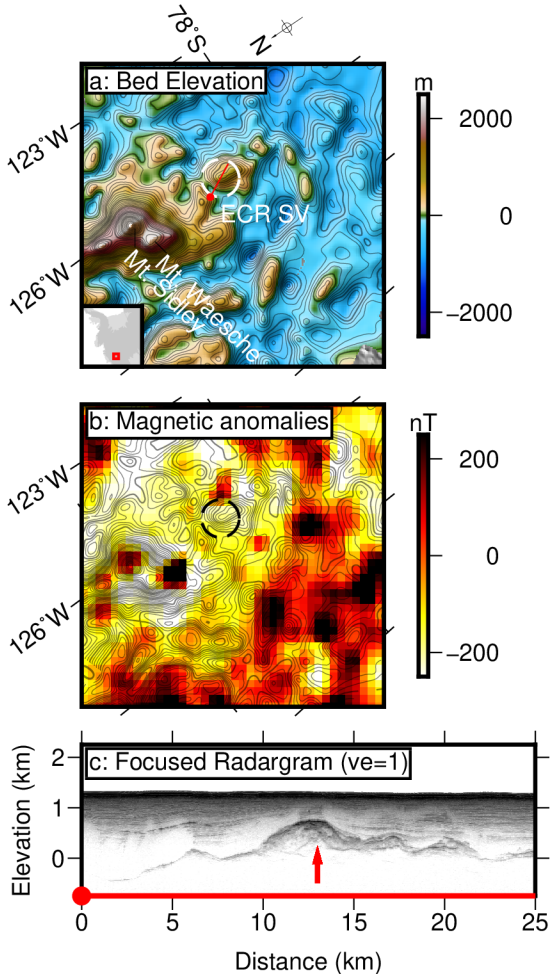

Figure 10: The Executive Committee Range Subglacial Volcano (ECR SV), overlying the magma chamber proposed by (Lough et al., 2013) a) bed elevation (compiled from (Blankenship et al., 2012) and (Young et al., 2017); red line shows location of radargram in panel c) where ball is the start of the line b) ADMAP-2 magnetic anomalies with bed elevation contours (Golynsky et al., 2018) showing offset magnetic anomaly. c) portion of focused radargram MBL/MKB2l/Y89a. Red arrow points to ECR SV.

The active subglacial volcano interpreted by *Lough et al., (2013)* was directly imaged as part of the Geophysical Investigation of Marie Byrd Land Lithospheric Evolution (GIMBLE) airborne geophysical program (*Young et al., 2017*) and corresponds to a subglacial topographic high ~ 1000 m above its surroundings (ECR SV, Fig. 10 a,c) and a 400 nT magnetic anomaly ((Lough et al., 2013), Fig. 10 b). GIMBLE also detected significant subglacial water to the south of the Executive Committee Range (*Young et al., 2015*).

While a significant englacial ash layer is imaged in this region (*Lough et al., 2013*), both the observation of tephra bands in a zone of ablating blue ice and the distribution of the ash layer in a wind-oriented streak south of the active subaerial Mount Waesche suggest the source is most probably Mount Waesche. Perhaps the strongest argument for a Mount Waesche source is the implausibility of an eruption from the deep long-period source venting ash to the surface.

Amundsen Sea Embayment Sector

The Amundsen Sea Embayment is located within the deepest region of WARS. It is bounded by thicker and higher elevation crustal blocks to the south, northeast, and northwest (EWM, eMBL, and TI respectively), and by the Siple Coast to the west. Within the Amundsen Sea Embayment's low and landward sloping bed flow some of the fastest-flowing, most rapidly changing ice streams on Earth currently at risk of rapid collapse (*Joughin et al., 2014; Mouginot et al., 2014*), which makes this sector of WAIS a main component in scenarios of rapid deglaciation.

In this sector of WAIS, geothermal flux can have a large impact on ice flow organization and ice stream basal sliding velocity through the production of subglacial melt water. Not only does geothermal flux play a key role on ice flow velocity; importantly, it can also potentially control ice flow initiation along ice divides.

Hudson Mountains subglacial edifice

Subglacial volcanic activity near the Hudson Mountains was identified by *Corr & Vaughan, (2008)* as the source of a bright, local englacial layer as imaged in radar data. The strong radar reflection covers an elliptical area of about 23,000 km^2. The source region for the tephra layer, which has not been overflown with airborne geophysical surveys, was identified using the layer's radar echo strength as a proxy for the tephra thickness and proximity to the volcanic center, and coincides with a subglacial topographic high close to the Hudson Mountains characterized by a complex pattern of positive magnetic anomalies (*Golynsky et al., 2018*). The layer depth dates the eruption at 207 BC ± 240 years, which matches strong and previously unattributed conductivity signals measured in two ice cores, Byrd Station and Siple Dome (*Corr & Vaughan, 2008; Hammer et al., 1997; Kurbatov et al., 2006*). *Rowley et al., (1986)* report anecdotal evidence of recent volcanic activity including a report of the "possible presence of steam" in 1974. However, the report of a possible eruption based on satellite data in 1985 (PR Kyle, cited by Rowley et al., 1990) is weakly founded and probably should be discounted (personal communication from John Smellie based on information provided by PR Kyle, March 2020).

Thwaites Glacier heat flow anomalies

Indirect evidence of elevated geothermal flux from airborne radar sounding data and a subglacial hydrologic model points to localized heat flow anomalies ~ 200 mW/m^2 within the Thwaites Glacier catchment (*Schroeder et al., (2014);* Fig. 1 and 11). High geothermal flux is postulated along the ice covered flanks of two subaerial volcanoes active within the last 50,000 years, (Mt. Takahe (*Palais et al., 1988*) and Mt. Frakes (*Wilch & McIntosh, 2002*)); over subglacial volcano Mt. Thiel; and possibly associated with two additional circular positive magnetic anomalies associated with subglacial edifices. The spatial distribution of these heat flow anomalies at the inception of tributaries and fast flowing ice streams is additional evidence of the potential impact of active volcanism on ice organization and ice sheet dynamics.

Discussion

We find that active subglacial volcanism identified in this chapter manifests near identified crustal and lithospheric boundary zones. In the Siple Coast sector, volcanism and heat flow anomalies are mostly associated with the southern edge of the WARS, and within 150 km of the crustal block boundary (Figure 11) with Mt. CASERTZ lying on the edge of a sharp crustal thickness boundary (Fig. 5 d). Fast moving ice streams may act to erode volcanic edifices in this

sector, biasing the observations. In addition, most of the radar data over this region is older incoherent data (*Blankenship et al., 2001*).

The sole identified active subglacial edifice in Marie Byrd Land (Fig 10) is again within 150 km of a crustal boundary but also lies in line with recently active volcanoes at the southern end of the Executive Committee Range (*Lough et al., 2013*). The Executive Committee Range, and its associated subglacial edifice, lie centered within the Marie Byrd Land Magnetic District (MMD), a broad region with suppressed magnetic anomalies surrounded by an intense magnetic front. We suggest that this crust has been modified by an underlying mantle hotspot, consistent with slow mantle velocities observed under the MMD (*Hansen et al., 2014*), and large isostatic anomalies derived from crustal thickness measurements (*Chaput et al., 2014; Winberry & Anandakrishnan, 2004)*.

The WAIS Divide and Amundsen sectors straddle the WARS, and the crustal thickness boundaries defined by gravity (Fig 11). Instead, these associations are more controlled by the magnetic crustal provinces defined by *Quartini (2018)*. The Amundsen sector is largely defined by the heat flow anomalies identified by *Schroeder et al., (2014)*; these heat flow anomalies are separated by the TMD, which was interpreted as old, unmodified Cretaceous lithosphere. Heat flow anomalies cluster along the eastern edge of the Marie Byrd Land crustal block, which coincides with the well defined boundary between the MMD and the TMD, as well as the recently active subaerial volcanoes Mt. Takahe and Mt. Frakes. Three heat flow anomalies are located in the PMD, with some associated with topography and large circular magnetic anomalies. Care must be taken in this interpretation, as the signal of excess geothermal flux in central Thwaites may be overwhelmed by the substantial frictional melting due to fast ice flow in this region.

Fast ice flow is not a factor for the WAIS Divide sector, which lies in the transition zone between the TMD and Central West Antarctica. Here the signal of high heat flow and edifice construction is most clearly preserved, due to a lack of glacial erosion. Ice thickness varies considerably here. An additional factor is the likely large degree of isostatic rebound in this region (see Table 2 for estimates of Airy isostatic rebound). In the event of a partial collapse of this region of the ice sheet in the last interglacial at 120,000 years ago (*DeConto & Pollard, 2016*), most of the edifices in the WAIS Divide sector would be expected to rebound close to sea level, leading to shallow submarine volcanic forms. If activity now indicated by high basal echo strengths and layer draw down extended into the last interglacial, hybrid forms could be observed.

Table 2. List of active subglacial volcanoes and heat flow anomalies in West Antarctica described in this study.

Feature	Coordinates	Ice thickness	Bed elevation	Rebounded	Crustal thickness	Ice flow velocity
Mt. CASERTZ Edifice[1]	81.88°S, 111.30°W	1791 m	-79 m	518 m	27.5 km	10 m yr^{-1}
KIS Subglacial Edifice[2]	82.00°S, 113.00°W	1816 m	-295 m	310 m	26.5 km	14 m yr^{-1}
Subglacial Lake Whillans	84.25°S, 153.50°W	799 m	-667 m	-400 m	25.6 km	350 m yr^{-1}

heatflow anomaly[3]						
WAIS Divide heatflow anomaly[4]	79.47°S, 112.09°W	3441 m	-1645 m	-498 m	22.4 km	12 m yr^{-1}
L′ Edifice[5]	78.08°S, 117.96°W	2537 m	-772 m	73 m	23.0 km	16 m yr^{-1}
H Fissure[5]	77.95°S, 118.24°W	2923 m	-1158 m	-183 m	23.1 km	5 m yr^{-1}
Central WAIS Caldera[6]	78.67°S, 114.50°W	2820 m	-1012 m	-72 m	22.5 km	8 m yr^{-1}
C′ Edifice[6]	79.12°S, 114.52°W	2540 m	-752 m	-51 m	22.5 km	8 m yr^{-1}
Mt. Thiel Edifice[7]	78.42°S, 111.33°W	1425 m	174 m	649 m	22.0 km	7 m yr^{-1}
ECR Edifice[8]	77.65°S, 126.77°W	726 m	2060 m	2303 m	27.6 km	3 m yr^{-1}
Hudson Mts Edifice[9]	74.67°S, 97.00°W	775 m	212 m	470 m	23.1 km	2 m yr^{-1}
Thwaites A hot spot[10]	78.23°S, 103.12°W	2220 m	-611 m	128 m	22.6 km	19 m yr^{-1}
Thwaites B hot spot[10]	77.93°S, 104.52°W	1986 m	-533 m	129 m	22.2 km	15 m yr^{-1}
Thwaites C heatflow anomaly[10]	78.77°S, 108.69°W	2333 m	-598 m	180 m	22.3 km	2 m yr^{-1}
Thwaites D heatflow anomaly[10]	78.42°S, 111.33°W	1424 m	175 m	649 m	22.1 km	8 m yr^{-1}
Thwaites E heatflow anomaly[10]	76.67°S, 115.86°W	3050 m	-1580 m	-563 m	23.2km	-*
Thwaites F heatflow anomaly[10]	76.57°S, 117.08°W	3068 m	-1525 m	-503 m	23.5 km	-*
Thwaites G heatflow anomaly[10]	79.22°S, 100.89°W	3000 m	-1041 m	-42 m	23.6 km	-*
Thwaites H heatflow anomaly[10]	76.32°S, 110.51°W	2139 m	-1021 m	-306 m	23.0 km	168 m yr^{-1}
Thwaites I heatflow anomaly[10]	76.73°S, 112.16°W	2671 m	-1388 m	-497 m	22.7 km	108 m yr^{-1}

Thwaites J heatflow anomaly[10]	76.60°S, 123.08°W	2808 m	-595 m	340 m	24.6 km	11 m yr^{-1}

[1](Blankenship et al., 1993); [2](Filina et al., 2008); [3](Fisher et al., 2015); [4](Clow et al., 2012); [5](Danque, 2008); [6](Behrendt et al., 1998); [7](Behrendt, 2013); [8](Lough et al., 2013); [9](Corr & Vaughan, 2008); [10](Schroeder et al., 2014); [11](Fretwell et al., 2013); [12]Airy isostatic rebound; [13](Chaput et al., 2014); [15](Rignot et al., 2014); *No data.

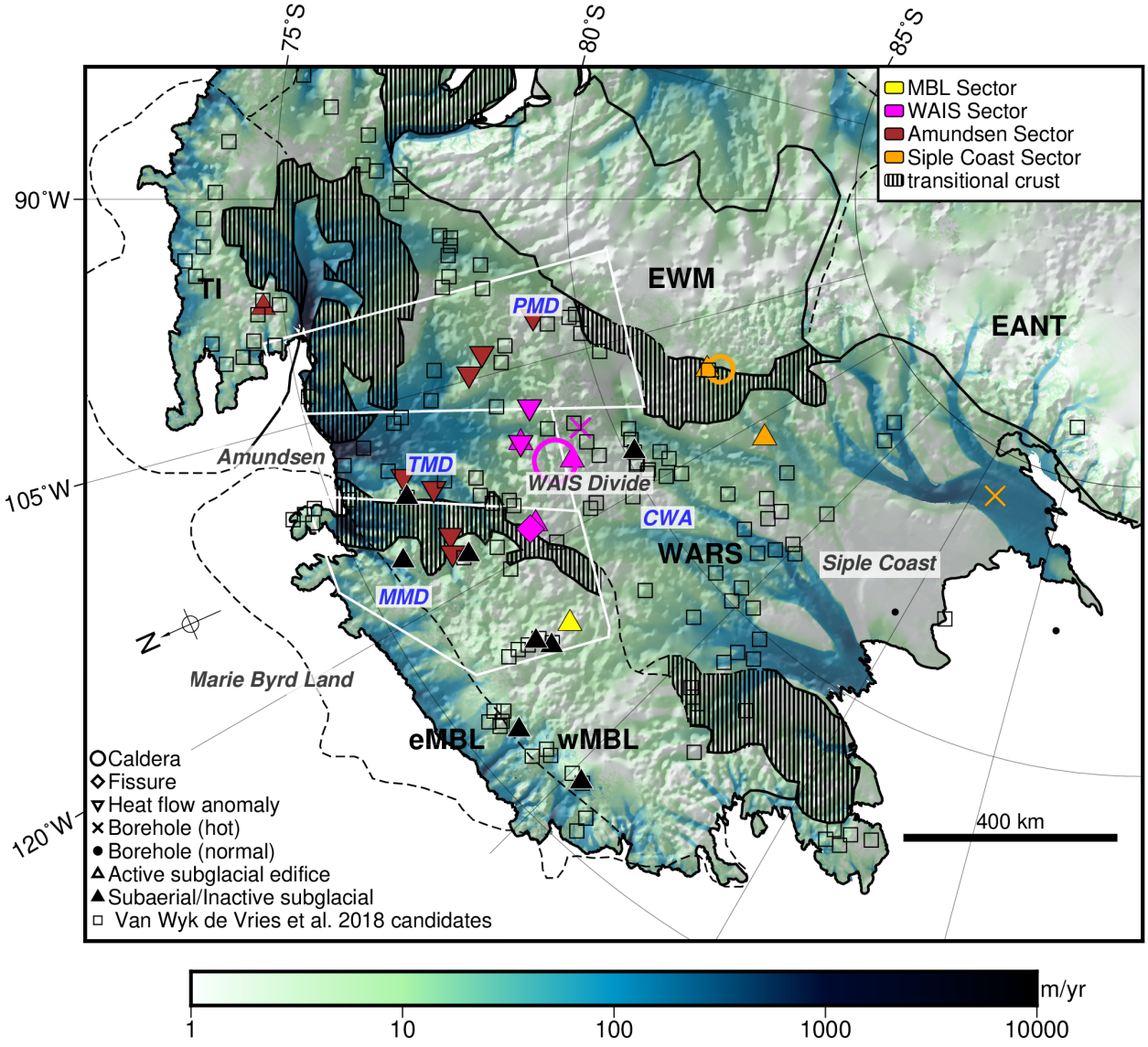

Figure 11: Distribution of proposed sites of active subglacial volcanism and proposed volcanic edifices over crustal boundaries identified by (Diehl et al., 2008) and (Quartini, 2018). Shading from the bed rock DTM used in this study; velocity overlay is from (Mouginot et al., 2019). Also shown are candidate volcanoes identified by van Wyk de Vries et al. (2018).

Conclusions

Active subglacial volcanism is identified throughout West Antarctica, within different geological and glaciological local contexts. The majority of active subglacial volcanic sites in West Antarctica concentrate along crustal boundaries and within central WARS, which are regions of thinned, rifted crust that have been tectonically reactivated during multiple stages of WARS formation (*Dalziel, 1992*). Subglacial volcanic sites also overlap with areas of relatively thick ice and slow ice surface flow, both of which are critical conditions for the preservation of volcanic records (*Behrendt et al., 1998*). However, other geological and glaciological considerations can explain the spatial distribution of active subglacial sites observed in West Antarctica. Factors such as crustal age and thickness can explain the lack of active subglacial volcanism within sectors characterized by thicker crust such as crustal blocks and the Siple Coast (*Chaput et al., 2014*). On the other hand, the lithosphere underlying Thwaites Glacier's main trunk is likely to have cooled, and volcanic activity in the area ceased since the last emplacement of basaltic wedges during the early mid-Mesozoic stages of WARS formation (*Gohl et al., 2013*).

Finally, the glaciological regimes in each sector impose biases to the preservation of subglacial volcanic records which can potentially prevent detection of volcanic activity even where present. Subglacial eruptions under thin ice produce more brittle and less consolidated deposits, such as hyaloclastites, compared to eruptions under the high pressure conditions of thicker ice columns, where more erosion-resistant pillow lava flows form (*Gudmundsson et al., 1997*). As a result, the products of volcanic activity under thinner ice columns are more prone to erosion and removal by the ice sheet (*Behrendt et al., 1998*). This is particularly relevant in regions of fast ice flow, such as the Siple Coast and main trunk of Thwaites Glacier. While Thwaites Glacier is a region of high driving stresses and thick ice, the Siple Coast ice streams are characterized by thin ice, making this a region particularly prone to loss of subglacial volcanic records.

By altering the ice's thermal structure and generating basal melt water, heterogeneous geothermal flux has the potential to affect ice dynamics in all sectors of West Antarctica where active subglacial volcanism is observed. Large areas of both West and East Antarctica have been surveyed but not yet searched for evidence of active subglacial volcanism and it is likely that further discoveries of active subglacial volcanism shall be made.

List of abbreviations

AGASEA: Airborne Geophysical Survey of the Amundsen Embayment
ANET-POLENET: Antarctic Polar Earth Observing Network
AP: Antarctic Peninsula
CASERTZ: Corridor Aerogeophysics of the South Eastern Ross Transect Zone
DEM: Digital Elevation Model
DLP: Deep Long Period
eMBL: Eastern Marie Byrd Land
EWM Ellsworth-Whitmore Mountains
GIMBLE: Geophysical Investigation of Marie Byrd Land Lithospheric Evolution
GPS: Global Positioning System
HiCARS: High Capability Radar Sounder
IPR: Ice penetrating radar
KIS: Kamb Ice Stream
MBL: Marie Byrd Land
MMD: Marie Byrd Land Magnetic District

MOA: Mosaic Of Antarctica
PMD: Pine Island Magnetic District
POLENET: Polar Earth Observing Network
SAR: Synthetic Aperture Radar
SLW: Subglacial Lake Whillans
TI: Thurston Island
TMD: Thwaites Magnetic District
UTIG: University of Texas Institute for Geophysics
WAIS: West Antarctic Ice Sheet
WARS: West Antarctic Rift System
WISSARD: Whillans Ice Stream Subglacial Access Research Drilling
wMBL: Western Marie Byrd Land

Acknowledgements

The authors thank the anonymous reviewers and the editor for their careful reading of our manuscript and their many insightful comments and suggestions.

This work was supported by the G. Unger Veltesen Foundation, a graduate fellowship from the University of Texas Institute for Geophysics, and NSF grant PLR-1043761. This is UTIG contribution ####.

Accardo, N. J., Wiens, D. A., Hernandez, S., Aster, R. C., Nyblade, A., Huerta, A., et al. (2014). Upper mantle seismic anisotropy beneath the West Antarctic Rift System and surrounding region from shear wave splitting analysis. *Geophysical Journal International*, *198*(1), 414–429. https://doi.org/10.1093/gji/ggu117

An, M., Wiens, D. A., Zhao, Y., Feng, M., Nyblade, A., Kanao, M., et al. (2015). Temperature, lithosphere-asthenosphere boundary, and heat flux beneath the Antarctic Plate inferred from seismic velocities. *Journal of Geophysical Research: Solid Earth*, *120*(12), 8720–8742. https://doi.org/10.1002/2015JB011917

Begeman, C. B., Tulaczyk, S. M., & Fisher, A. T. (2017). Spatially variable geothermal heat flux in West Antarctica: Evidence and implications. *Geophysical Research Letters*, *44*(19), 9823–9832. https://doi.org/10.1002/2017GL075579

Behrendt, J. C. (1964). Distribution of narrow-width magnetic anomalies in Antarctica. *Science*, *144*, 995–999. https://doi.org/10.1126/science.144.3621.993

Behrendt, J. C. (2013). The aeromagnetic method as a tool to identify Cenozoic magmatism in the West Antarctic Rift System beneath the West Antarctic Ice Sheet — A review; Thiel subglacial volcano as possible source of the ash layer in the WAISCORE. *Tectonophysics*, *585*(0), 124–136. https://doi.org/10.1016/j.tecto.2012.06.035

Behrendt, J. C., LeMasurier, W. E., Cooper, A. K., Tessensohn, F., Tréhu, A., & Damaske, D. (1991). Geophysical studies of the West Antarctic Rift System. *Tectonics*, *10*(6), 1257–1273. Retrieved from http://dx.doi.org/10.1029/91TC00868

Behrendt, J. C., Blankenship, D. D., Finn, C. A., Bell, R. E., Sweeney, R. E., Hodge, S. M., & Brozena, J. M. (1994). CASERTZ aeromagnetic data reveal late Cenozoic flood basalts(?) in the

West Antarctic rift system. *Geology*, *22*(6), 527–530. Retrieved from http://geology.geoscienceworld.org/cgi/content/abstract/22/6/527

Behrendt, J. C., Blankenship, D. D., Damaske, D., & Cooper, A. K. (1995). Glacial removal of late Cenozoic subglacially emplaced volcanic edifices by the West Antarctic ice sheet. *Geology*, *23*(12), 1111–1114.

Behrendt, J. C., Saltus, R., Damaske, D., McCafferty, A., Finn, C. A., Blankenship, D., & Bell, R. E. (1996). Patterns of late Cenozoic volcanic and tectonic activity in the West Antarctic rift system revealed by aeromagnetic surveys. *Tectonics*, *15*, 660–676. https://doi.org/10.1029/95TC03500

Behrendt, J. C., Finn, C. A., Blankenship, D., & Bell, R. E. (1998). Aeromagnetic evidence for a volcanic caldera(?) complex beneath the divide of the West Antarctic Ice Sheet. *Geophysical Research Letters*, *25*, 4385–4388.

Behrendt, J. C., Blankenship, D. D., Morse, D. L., Finn, C. A., & Bell, R. E. (2002). Subglacial volcanic features beneath the West Antarctic Ice Sheet interpreted from aeromagnetic and radar ice sounding. *Geological Society, London, Special Publications; 202*, 337–355. https://doi.org/10.1144/GSL.SP.2002.202.01.17

Behrendt, J. C., Finn, C. A., & Blankenship, D. D. (2006). Examples of Models Fit to Magnetic Anomalies Observed Over Subaerial, Submarine, and Subglacial Volcanoes in the West Antarctic Rift System. *AGU Fall Meeting Abstracts*, 2006.

Bhattacharyya, B., & Leu, L.-K. (1975). Analysis of magnetic anomalies over Yellowstone National Park: mapping of Curie point isothermal surface for geothermal reconnaissance. *Journal of Geophysical Research*, *80*(32), 4461–4465.

Bingham, R. G., & Siegert, M. J. (2007). Radio-echo sounding over polar ice masses. *Journal of Environmental and Engineering Geophysics*, *12*(1), 47–62. https://doi.org/10.2113/JEEG12.1.47

Björnsson, H. (2003). Subglacial lakes and jökulhlaups in Iceland. *Global and Planetary Change*, *35*(3-4), 255–271.

Blankenship, D. D., Bell, R. E., Hodge, S. M., Brozena, J. M., Behrendt, J. C., & Finn, C. A. (1993). Active volcanism beneath the West Antarctic ice sheet and implications for ice-sheet stability. *Nature*, *361*, 526–529.

Blankenship, D. D., Morse, D., Finn, C. A., Bell, R. E., Peters, M. E., Kempf, S. D., et al. (2001). Geological controls on the initiation of rapid basal motion for West Antarctic Ice Streams: A geophysical perspective including new airborne radar sounding and laser altimetry results. In R. B. Alley & R. A. Bindschadler (Eds.), *The west antarctic ice sheet: Behavior and environment* (Vol. 77, pp. 105–121). American Geophysical Union.

Blankenship, D. D., Young, D. A., Holt, J. W., & Kempf, S. D. (2012). *AGASEA ice thickness profile data from the Amundsen Sea Embayment, Antarctica* (Digital media). Boulder, Colorado USA: National Snow; Ice Data Center. https://doi.org/10.7265/N5W95730

Buizert, C., Cuffey, K., Severinghaus, J., Baggenstos, D., Fudge, T., Steig, E., et al. (2015). The WAIS Divide deep ice core WD2014 chronology-part 1: Methane synchronization (68-31 ka BP) and the gas age-ice age difference. *Climate of the Past*, *11*(2), 153.

Cavitte, M. G. P., Blankenship, D. D., Young, D. A., Schroeder, D. M., Parrenin, F., Meur, E. L., et al. (2016). Deep radiostratigraphy of the East Antarctic Plateau: connecting the Dome C and Vostok ice core sites. *Journal of Glaciology*, 1–12. https://doi.org/10.1017/jog.2016.11

Chaput, J., Aster, R. C., Huerta, A., Sun, X., Lloyd, A., Wiens, D., et al. (2014). The crustal thickness of West Antarctica. *Journal of Geophysical Research*, *119*(1), 378-395. https://doi.org/10.1002/2013JB010642

Christianson, K., Jacobel, R. W., Horgan, H. J., Anandakrishnan, S., & Alley, R. B. (n.d.). Subglacial Lake Whillans —Ice-penetrating radar and GPS observations of a shallow active reservoir beneath a West Antarctic ice stream. *Earth and Planetary Science Letters*, *331–332*(0), 237–245. Retrieved from http://www.sciencedirect.com/science/article/pii/S0012821X12001276

Christoffersen, P., Bougamont, M., Carter, S. P., Fricker, H. A., & Tulaczyk, S. (2014). Significant groundwater contribution to Antarctic ice streams hydrologic budget. *Geophysical Research Letters*, *41*(6), 2003–2010. https://doi.org/10.1002/2014GL059250

Clow, G., Cuffey, K., & Waddington, E. (2012). High heat-flow beneath the central portion of the west antarctic ice sheet. *AGU fall meeting abstracts 2012*.

Corr, H. F. J., & Vaughan, D. G. (2008). A recent volcanic eruption beneath the West Antarctic ice sheet. *Nature Geoscience*, *1*, 122–125. https://doi.org/10.1038/ngeo106

Dalziel, I. W. D. (1992). Antarctica: a tale of Two Supercontinents? *Annual Review of Earth and Planetary Sciences*, *20*, 501–526. https://doi.org/10.1146/annurev.ea.20.050192.002441

Dalziel, I. W. D., & Lawver, L. A. (2001). The lithospheric setting of the West Antarctic Ice Sheet. In R. B. Alley & R. Bindschadler (Eds.), *The west antarctic ice sheet: Behavior and environment* (Vol. 77, pp. 13–44). American Geophysical Union.

Damiani, T. M., Jordan, T. A., Ferraccioli, F., Young, D. A., & Blankenship, D. D. (2014). Variable crustal thickness beneath Thwaites Glacier revealed from airborne gravimetry, possible implications for geothermal heat flux in West Antarctica. *Earth and Planetary Science Letters*, *407*(0), 109–122. https://doi.org/http://dx.doi.org/10.1016/j.epsl.2014.09.023

Danque, H. A. (2008). *Subglacial West Antarctic volcanoes defined by aerogeophysical data and the potential for associated hydrothermal systems* (Master's thesis, University of Texas at Austin), 112p.

Davies, J. H. (2013). Global map of solid Earth surface heat flow. *Geochemistry, Geophysics, Geosystems*, *14*(10), 4608–4622. https://doi.org/10.1002/ggge.20271

DeConto, R. M., & Pollard, D. (2016). Contribution of Antarctica to past and future sea-level rise. *Nature*, *531*(7596), 591–597. Retrieved from http://dx.doi.org/10.1038/nature17145

Diehl, T. M. (2008). *Gravity analyses for the crustal structure and subglacial geology of West Antarctica, particularly beneath Thwaites Glacier* (Doctoral dissertation, University of Texas at Austin), 209 p.

Diehl, T. M., Holt, J. W., Blankenship, D. D., Young, D. A., Jordan, T. A., & Ferraccioli, F. (2008). First airborne gravity results over the Thwaites Glacier catchment, West Antarctica. *Geochemistry, Geophysics, Geosystems*, *8*(Q04011). https://doi.org/10.1029/2007GC001878

Emry, E., Nyblade, A. A., Julià, J., Anandakrishnan, S., Aster, R., Wiens, D. A., et al. (2015). The mantle transition zone beneath West Antarctica: seismic evidence for hydration and thermal upwellings. *Geochemistry, Geophysics, Geosystems*, *16*(1), 40–58.

Engelhardt, H. (2004a). Ice temperature and high geothermal flux at Siple Dome, West Antarctica, from borehole measurements. *Journal of Glaciology*, *50*(169), 251–256. https://doi.org/doi:10.3189/172756504781830105

Engelhardt, H. (2004b). Thermal regime and dynamics of the West Antarctic ice sheet. *Annals of Glaciology*, *39*(1), 85–92. https://doi.org/10.3189/172756404781814203

Fahnestock, M., Abdalati, W., Joughin, I., Brozena, J., & Gogineni, P. (2001). High geothermal heat flow, basal melt, and the origin of rapid ice flow in central Greenland. *Science*, *294*(5550), 2338–2342. Retrieved from http://www.sciencemag.org/cgi/content/abstract/294/5550/2338

Filina, I. Y., Blankenship, D. D., Thoma, M., Lukin, V. V., Masolov, V. N., & Sen, M. K. (2008). New 3D bathymetry and sediment distribution in Lake Vostok: Implication for pre-glacial origin and numerical modeling of the internal processes within the lake. *Earth and Planetary Science Letters*, *276*(1-2), 106–114. https://doi.org/10.1016/j.epsl.2008.09.012

Fisher, A. T., Mankoff, K. D., Tulaczyk, S. M., Tyler, S. W., & Foley, N. (2015). High geothermal heat flux measured below the West Antarctic Ice Sheet. *Science Advances*, *1*(6). https://doi.org/10.1126/sciadv.1500093

Fretwell, P., Pritchard, H. D., Vaughan, D. G., Bamber, J. L., Barrand, N. E., Bell, R., et al. (2013). Bedmap2: Improved ice bed, surface and thickness datasets for Antarctica. *The Cryosphere*, *7*, 375–393. https://doi.org/10.5194/tc-7-375-2013

Fricker, H. A., & Padman, L. (2012). Thirty years of elevation change on Antarctic Peninsula ice shelves from multimission satellite radar altimetry. *Journal of Geophysical Research*, *117*(C2), n/a–n/a. https://doi.org/10.1029/2011JC007126

Fudge, T. J., Steig, E. J., Markle, B. R., Schoenemann, S. W., Ding, Q., Taylor, K. C., et al. (n.d.). Onset of deglacial warming in West Antarctica driven by local orbital forcing. *Nature*, *500*(7463), 440–444. Retrieved from http://dx.doi.org/10.1038/nature12376

Fujita, S., Maeno, H., Uratsuka, S., Furukawa, T., Mae, S., Fujii, Y., & Watanabe, O. (1999). Nature of radio echo layering in the Antarctic ice sheet detected by a two-frequency experiment. *Journal of Geophysical Research*, *104*(B6), 13049–13060. https://doi.org/10.1029/1998JB900034

Gohl, K., Denk, A., Eagles, G., & Wobbe, F. (2013). Deciphering tectonic phases of the Amundsen Sea Embayment shelf, West Antarctica, from a magnetic anomaly grid. *Tectonophysics*, *585*(0), 113–123. https://doi.org/10.1016/j.tecto.2012.06.036

Golynsky, A. V., Ferraccioli, F., Hong, J. K., Golynsky, D. A., Frese, R. R. B. von, Young, D. A., et al. (2018). New magnetic anomaly map of the Antarctic. *Geophysical Research Letters, 45(13), 6437-6449*.

Gudmandsen, P. (1971). Electromagnetic probing of ice. In J. R. Wait (Ed.), *Electromagnetic probing in geophysics* (pp. 321–348). Colorado: Golem Press.

Gudmundsson, M. T. (1996). Ice-volcano interaction at the subglacial Grímsvötn Volcano, Iceland. *Glaciers, Ice Sheets and Volcanoes: A Tribute to Mark F. Meier*, 34-40.

Gudmundsson, M. T., & Högnadóttir, T. (2007). Volcanic systems and calderas in the Vatnajökull region, central iceland: Constraints on crustal structure from gravity data. *Journal of Geodynamics*, *43*(1), 153–169.

Gudmundsson, M. T., Sigmundsson, F., & Björnsson, H. (1997). Ice–volcano interaction of the 1996 Gjálp subglacial eruption, vatnajökull, iceland. *Nature*, *389*(6654), 954-957.

Hammer, C. U., Clausen, H. B., & Langway, J., C. C. (1997). 50,000 years of recorded global volcanism. *Climatic Change*, *35*(1), 1–15. https://doi.org/10.1023/A:1005344225434

Hansen, S. E., Graw, J. H., Kenyon, L. M., Nyblade, A. A., Wiens, D. A., Aster, R. C., et al. (2014). Imaging the Antarctic mantle using adaptively parameterized P-wave tomography: evidence for heterogeneous structure beneath West Antarctica. *Earth and Planetary Science Letters*, *408*(0), 66–78. https://doi.org/http://dx.doi.org/10.1016/j.epsl.2014.09.043

Hawkesworth, C. J., Blake, S., Evans, P., Hughes, R., Macdonald, R., Thomas, L. E., et al. (2000). Time scales of crystal fractionation in magma chambers—integrating physical, isotopic and geochemical perspectives. *Journal of Petrology*, *41*(7), 991–1006. https://doi.org/10.1093/petrology/41.7.991

Heeszel, D. S., Wiens, D. A., Anandakrishnan, S., Aster, R. C., Dalziel, I. W. D., Huerta, A. D., et al. (2016). Upper mantle structure of central and West Antarctica from array analysis of Rayleigh wave phase velocities. *Journal of Geophysical Research: Solid Earth*, *121*(3), 1758–1775. https://doi.org/10.1002/2015JB012616

Hindmarsh, R. C., Leysinger Vieli, G. J., Raymond, M. J., & Gudmundsson, G. H. (2006). Draping or overriding: The effect of horizontal stress gradients on internal layer architecture in ice sheets. *Journal of Geophysical Research: Earth Surface*, *111*(F2). **https://doi.org/10.1029/2005JF000309**

Holt, J. W., Peters, M. E., Kempf, S. D., Morse, D. L., & Blankenship, D. D. (2006). Echo source discrimination in single-pass airborne radar sounding data from the Dry Valleys, Antarctica: Implications for orbital sounding of Mars. *Journal of Geophysical Research*, *111*(E10). https://doi.org/10.1029/2005JE002525

Holt, J. W., Blankenship, D. D., Morse, D. L., Young, D. A., Peters, M. E., Kempf, S. D., et al. (2006). New boundary conditions for the West Antarctic ice sheet: Subglacial topography of the Thwaites and Smith Glacier catchments. *Geophysical Research Letters*, *33*(L09502). https://doi.org/10.1029/2005GL025561

Howat, I. M., Porter, C., Smith, B. E., Noh, M.-J., & Morin, P. (2019). The reference elevation model of Antarctica. *The Cryosphere*, *13*(2), 665–674. https://doi.org/10.5194/tc-13-665-2019

Iverson, N. A., Lieb-Lappen, R., Dunbar, N. W., Obbard, R., Kim, E., & Golden, E. (2017). The first physical evidence of subglacial volcanism under the West Antarctic Ice Sheet. *Scientific Reports*, *7*(1), 11457.

Jacobel, R. W., Gades, A. M., Gottschling, D. L., Hodge, S. M., & Wright, D. L. (1993). Interpretation of radar-detected internal layer folding in West Antarctic ice streams. *Journal of Glaciology*, *39*(133), 528–537.

Jankowski, E. J., & Drewry, D. J. (1981). The structure of West Antarctica from geophysical studies. *Nature*, *291*, 17–21. Retrieved from http://dx.doi.org/10.1038/291017a0

Joughin, I., Smith, B. E., & Medley, B. (2014). Marine ice sheet collapse potentially under way for the Thwaites Glacier basin, West Antarctica. *Science*, *344*(6185), 735–738. https://doi.org/10.1126/science.1249055

Kurbatov, A. V., Zielinski, G. A., Dunbar, N. W., Mayewski, P. A., Meyerson, E. A., Sneed, S. B., & Taylor, K. C. (2006). A 12,000 year record of explosive volcanism in the Siple Dome Ice Core, West Antarctica. *Journal of Geophysical Research: Atmospheres*, *111*(D12). https://doi.org/10.1029/2005JD006072

LeMasurier, W. E. (2006). What supports the Marie Byrd Land Dome? An evaluation of potential uplift mechanisms in a continental rift system. In D. K. Fütterer, D. Damaske, G. Kleinschmidt, H. Miller, & F. Tessensohn (Eds.), *Antarctica contributions to global earth sciences* (pp. 299–302). Berlin Heidelberg New York: Springer-Verlag. Retrieved from http://dx.doi.org/10.1007/3-540-32934-X_37

LeMasurier, W. E. (2008). Neogene extension and basin deepening in the West Antarctic rift inferred from comparisons with the East African rift and other analogs. *Geology*, *36*(3), 247–250. https://doi.org/10.1130/G24363A.1

LeMasurier, W. E., & Rex, D. C. (1989). Evolution of linear volcanic ranges in Marie Byrd Land, West Antarctica. *Journal of Geophysical Research*, *94*(B6), 7223–7236.

Leuschen, C., & Allen, C. (2011). *IceBridge MCoRDS L2 Ice Thickness* (Digital media). Boulder, Colorado USA: NASA DAAC at the National Snow and Ice Data Center. Retrieved from http://nsidc.org/data/irmcr2.html

Lloyd, A. J., Wiens, D. A., Nyblade, A. A., Anandakrishnan, S., Aster, R. C., Huerta, A. D., et al. (2015). A seismic transect across West Antarctica: Evidence for mantle thermal anomalies beneath the Bentley Subglacial Trench and the Marie Byrd Land dome. *Journal of Geophysical Research: Solid Earth*, 120(12), 8439-8460. https://doi.org/10.1002/2015JB012455

Lough, A. C., Wiens, D. A., Barcheck, C. G., Anandakrishnan, S., Aster, R. C., Blankenship, D. D., et al. (2013). Seismic detection of an active subglacial magmatic complex in Marie Byrd Land, Antarctica. *Nature Geoscience*, *6*, 1031–1035. https://doi.org/10.1038/ngeo1992

Maccaferri, F., Rivalta, E., Keir, D., & Acocella, V. (2014). Off-rift volcanism in rift zones determined by crustal unloading. *Nature Geosciences*, *7*, 297–300. https://doi.org/10.1038/ngeo2110

Matsuoka, K. (2011). Pitfalls in radar diagnosis of ice-sheet bed conditions: Lessons from englacial attenuation models. *Geophysical Research Letters*, *38*(5). https://doi.org/10.1029/2010GL046205

McConnell, J. R., Burke, A., Dunbar, N. W., Köhler, P., Thomas, J. L., Arienzo, M. M., et al. (2017). Synchronous volcanic eruptions and abrupt climate change ~17.7 ka plausibly linked by

stratospheric ozone depletion. *Proceedings of the National Academy of Sciences*, *114*(38), 10035–10040. https://doi.org/10.1073/pnas.1705595114

Morse, D. L., Blankenship, D. D., Waddington, E. D., & Neumann., T. A. (2002). A site for deep ice coring in West Antarctica: Results from aerogeophysical surveys and thermo-kinematic modeling. *Annals of Glaciology*, *35*, 36–44.

Mouginot, J., Rignot, E., & Scheuchl, B. (2014). Sustained increase in ice discharge from the Amundsen Sea Embayment, West Antarctica, from 1973 to 2013. *Geophysical Research Letters*, *41*(5), 1576–1584. https://doi.org/10.1002/2013GL059069

Mouginot, J., Rignot, E., & Scheuchl, B. (2019). Continent-wide, interferometric SAR phase, mapping of Antarctic ice velocity. *Geophysical Research Letters*, *46*(16), 9710–9718. https://doi.org/10.1029/2019GL083826

Nereson, N. A., Raymond, C. F., Waddington, E. D., & Jacobel, R. W. (1998). Recent migration of Siple Dome ice divide, West Antarctica. *Journal of Glaciology*, *44*(148), 643–652.

Nichols, M., Malone, S., Moran, S., Thelen, W., & Vidale, J. (2011). Deep long-period earthquakes beneath Washington and Oregon volcanoes. *Journal of Volcanology and Geothermal Research*, *200*(3-4), 116–128.

Okubo, P. G., & Wolfe, C. J. (2008). Swarms of similar long-period earthquakes in the mantle beneath Mauna Loa Volcano. *Journal of Volcanology and Geothermal Research*, *178*(4), 787–794.

Palais, J. M., Kyle, P. R., McIntosh, W. C., & Seward, D. (1988). Magmatic and phreatomagmatic volcanic activity at Mt. Takahe, West Antarctica, based on tephra layers in the Byrd ice core and field observations at Mt. Takahe. *Journal of Volcanology and Geothermal Research*, *35*(4), 295–317. https://doi.org/10.1016/0377-0273(88)90025-X

Paulsen, T. S., & Wilson, T. J. (2010). Evolution of neogene volcanism and stress patterns in the glaciated West Antarctic Rift, Marie Byrd Land, Antarctica. *Journal of the Geological Society*, *167*, 401–416. https://doi.org/10.1144/0016-76492009-044

Peters, M. E., Blankenship, D. D., & Morse, D. L. (2005). Analysis techniques for coherent airborne radar sounding: Application to West Antarctic ice streams. *Journal of Geophysical Research*, *110*(B06303). https://doi.org/10.1029/2004JB003222

Peters, M. E., Blankenship, D. D., Carter, S. P., Young, D. A., Kempf, S. D., & Holt, J. W. (2007). Along-track focusing of airborne radar sounding data from West Antarctica for improving basal reflection analysis and layer detection. *IEEE Transactions on Geoscience and Remote Sensing*, *45*(9), 2725–2736. https://doi.org/10.1109/TGRS.2007.897416

Pittard, M. L., Galton-Fenzi, B. K., Roberts, J. L., & Watson, C. S. (2016). Organization of ice flow by localized regions of elevated geothermal heat flux. *Geophysical Research Letters*, *43*, 3342–3350. https://doi.org/10.1002/2016GL068436

Power, J., Stihler, S., White, R., & Moran, S. (2004). Observations of deep long-period (DLP) seismic events beneath Aleutian arc volcanoes; 1989–2002. *Journal of Volcanology and Geothermal Research*, *138*(3-4), 243–266.

Price, S. F., Bindschadler, R. A., Hulbe, C. L., & Joughin, I. R. (2001). Post-stagnation behavior in the upstream regions of Ice Stream C, West Antarctica. *Journal of Glaciology*, *47*(157), 283–294. https://doi.org/https://doi.org/10.3189/172756501781832232

Quartini, E. (2018). *The distribution of geothermal flux in West Antarctica* (Doctoral dissertation, University of Texas at Austin), 109 p.

Raymond, C. F. (1983). Deformation in the vicinity of ice divides. *Journal of Glaciology*, *29*(103), 357–373.

Retzlaff, R., & Bentley, C. R. (1993). Timing of stagnation of Ice Stream C, West Antarctica, from short-pulse radar studies of buried surface crevasses. *Journal of Glaciology*, *39*(133), 553–561. https://doi.org/10.3189/S0022143000016440

Rignot, E., Mouginot, J., Morlighem, M., Seroussi, H., & Scheuchl, B. (2014). Widespread, rapid grounding line retreat of Pine Island, Thwaites, Smith, and Kohler glaciers, West Antarctica, from 1992 to 2011. *Geophysical Research Letters*, *41*(10), 3502–3509. https://doi.org/10.1002/2014GL060140

Rowley, P. D., Thomson, J. W., Smellie, J. L., Laudon, T. S., La Prade, K. E., & LeMasurier, W. E. (1986). C. Alexander island, Palmer Island, and Ellsworth Land. In *Volcanoes of the antarctic plate and southern oceans* (pp. 256–301). American Geophysical Union (AGU). https://doi.org/10.1029/AR048p0256

Rowley, P.D., Laudon, T.S., La Prade, K.E. and LeMasurier, W.E. 1990. Hudson Mountains. In LeMasurier, W.E. and Thomson, J.W. (eds) Volcanoes of the Antarctic plate and southern Oceans. American Geophysical Union, Antarctic Research Series, 48, pp. 289-293.

Scambos, T. A., Haran, T. M., Fahnestock, M. A., Painter, T. H., & Bohlander, J. (2007). MODIS-based Mosaic of Antarctica (MOA) data sets: Continent-wide surface morphology and snow grain size. *Remote Sensing of Environment*, *111*(2-3), 242–257. https://doi.org/10.1016/j.rse.2006.12.020

Scheinert, M., Ferraccioli, F., Schwabe, J., Bell, R., Studinger, M., Damaske, D., et al. (2016). New Antarctic gravity anomaly grid for enhanced geodetic and geophysical studies in Antarctica. *Geophysical Research Letters*, *43*, 600–610. https://doi.org/10.1002/2015GL067439

Schmidt, B. E., Blankenship, D. D., Patterson, G. W., & Schenk, P. M. (2011). Active formation of "chaos terrain" over shallow subsurface water on Europa. *Nature*, *479*, 502–505. https://doi.org/10.1038/nature10608

Schoof, C. (2007). Ice sheet grounding line dynamics: Steady states, stability, and hysteresis. *Journal of Geophysical Research*, *112*(F03S28). https://doi.org/10.1029/2006JF000664

Schroeder, D. M., Blankenship, D. D., & Young, D. A. (2013). Evidence for a water system transition beneath Thwaites Glacier, West Antarctica. *Proceedings of the National Academy of Sciences*, 1–4. https://doi.org/10.1073/pnas.1302828110

Schroeder, D. M., Blankenship, D. D., Young, D. A., & Quartini, E. (2014). Evidence for elevated and spatially variable geothermal flux beneath the West Antarctic Ice Sheet. *Proceedings of the National Academies of Science*, *111*(25), 9070–9072. https://doi.org/10.1073/pnas.1405184111

Schroeder, D. M., Blankenship, D. D., Raney, R. K., & Grima, C. (2015). Estimating subglacial water geometry using radar bed echo specularity: Application to Thwaites Glacier, West Antarctica. *IEEE Geoscience and Remote Sensing Letters*, *12*(3), 443–447. https://doi.org/10.1109/LGRS.2014.2337878

Schroeder, D. M., Grima, C., & Blankenship, D. D. (2016). Evidence for variable grounding zone extent and shear margin bed conditions across Thwaites Glacier, West Antarctica. *Geophysics*, *81*(1), WA35–WA43. https://doi.org/10.1190/geo2015-0122.1

Sergienko, O. V., Creyts, T. T., & Hindmarsh, R. C. A. (2014). Similarity of organized patterns in driving and basal stresses of Antarctic and Greenland ice sheets beneath extensive areas of basal sliding. *Geophysical Research Letters*, *41*(11), 3925–3932. https://doi.org/10.1002/2014GL059976

Siegert, M. J., Welch, B., Morse, D., Vieli, A., Blankenship, D. D., Joughin, I., et al. (2004). Ice flow direction change in interior West Antarctica. *Science*, *305*(5692), 1948–1951. https://doi.org/10.1126/science.1101072

Singer, B. S. (2014). A quaternary geomagnetic instability time scale. *Quaternary Geochronology*, *21*, 29–52. https://doi.org/https://doi.org/10.1016/j.quageo.2013.10.003

Singer, B. S., Guillou, H., Jicha, B. R., Laj, C., Kissel, C., Beard, B. L., & Johnson, C. M. (2009). $^{40}Ar/^{39}ar$, k–ar and ^{230}th–^{238}u dating of the Laschamp excursion: A radioisotopic tie-point for ice core and climate chronologies. *Earth and Planetary Science Letters*, *286*(1), 80–88. https://doi.org/https://doi.org/10.1016/j.epsl.2009.06.030

Smellie, J. (2000). Subglacial eruptions. In H. Sigurdsson, B. Houghton, H. Rymer, J. Stix, & S. McNutt (Eds.), *The encyclopedia of volcanoes* (pp. 403–416).

Smellie, J. L. (2006). The relative importance of supraglacial versus subglacial meltwater escape in basaltic subglacial tuya eruptions: An important unresolved conundrum. *Earth-Science Reviews*, *74*(3-4), 241–268. Retrieved from http://www.sciencedirect.com/science/article/B6V62-4HNSPRP-2/2/8f782ab0badd6ffb06a6be89e618f601

Smith, R. B., & Braile, L. W. (1994). The Yellowstone hotspot. *Journal of Volcanology and Geothermal Research*, *61*(3-4), 121–187.

Spector, P., Stone, J., Pollard, D., Hillebrand, T., Lewis, C., & Gombiner, J. (2018). West Antarctic sites for subglacial drilling to test for past ice-sheet collapse. *The Cryosphere*, *12*(8), 2741–2757. https://doi.org/10.5194/tc-12-2741-2018

Stevens, N. T., Parizek, B. R., & Alley, R. B. (2016). Enhancement of volcanism and geothermal heat flux by ice-age cycling: A stress modeling study of Greenland. *Journal of Geophysical Research: Earth Surface*, *121*, 1456–1471. https://doi.org/10.1002/2016JF003855

Sweeney, R. E., Finn, C. A., Blankenship, D. D., Bell, R. E., & Behrendt, J. C. (1999). *Central West Antarctica aeromagnetic data: A web site for distribution of data and maps* (Open File Report No. 99-420). Denver, CO: U.S. Geological Survey. Retrieved from http://pubs.usgs.gov/of/1999/ofr-99-0420/cwantarctica.html

Turcotte, D., & Schubert, G. (2014). *Geodynamics*. Cambridge University Press, 472 p.

van Wyk de Vries, M., Bingham, R. G., & Hein, A. S. (2018). A new volcanic province: An inventory of subglacial volcanoes in West Antarctica. *Geological Society, London, Special Publications*, *461*(1), 231–248. https://doi.org/10.1144/SP461.7

Vaughan, D. G., Corr, H. F., Doake, C. S., & Waddington, E. D. (1999). Distortion of isochronous layers in ice revealed by ground-penetrating radar. *Nature*, *398*(6725), 323.

Vaughan, D. G., Corr, H. F. J., Ferraccioli, F., Frearson, N., O'Hare, A., Mach, D., et al. (2006). New boundary conditions for the West Antarctic Ice Sheet: Subglacial topography beneath Pine Island Glacier. *Geophysical Research Letters*, *33*(L09501). https://doi.org/10.1029/2005GL025588

Vogel, S. W., & Tulaczyk, S. M. (2006). Ice-dynamical constraints on the existence and impact of subglacial volcanism on West Antarctic ice sheet stability. *Geophysical Research Letters*, *33*(23), L23502. https://doi.org/10.1029/2006GL027345

Vogel, S. W., Tulaczyk, S. M., Carter, S. P., Renne, P., & Turrin, B. (2006). Geologic constraints on the existence and distribution of West Antarctic subglacial volcanism. *Geophysical Research Letters*, *33*(23), L23501. https://doi.org/10.1029/2006GL027344

Weertman, J. (1974). Stability of the junction of an ice sheet and ice shelf. *Journal of Glaciology*, *13*(67), 3–11.

Whillans, I. M. (1976). Radio-echo layers and the recent stability of the West Antarctic ice sheet. *Nature*, *264*(5582), 152.

Wilch, T. I., & McIntosh, W. C. (2002). Lithofacies analysis and $^{40}Ar/^{39}Ar$ geochronology of ice-volcano interactions at Mt. Murphy and the Crary Mountains, Marie Byrd Land, Antarctica. *Geological Society, London, Special Publications*, *202*(1), 237–253. https://doi.org/10.1144/GSL.SP.2002.202.01.12

Wilson, D. S., & Luyendyk, B. P. (2009). West antarctic paleotopography estimated at the Eocene-Oligocene climate transition. *Geophysical Research Letters*, *36*(16). https://doi.org/10.1029/2009GL039297

Winberry, J. P., & Anandakrishnan, S. (2004). Crustal structure of the West Antarctic rift system and Marie Byrd Land hotspot. *Geology*, *32*(11), 977–980. Retrieved from http://geology.geoscienceworld.org/cgi/content/abstract/32/11/977

Young, D. A., Schroeder, D. M., Blankenship, D. D., Kempf, S. D., & Quartini, E. (2015). The distribution of basal water between Antarctic subglacial lakes from radar sounding. *Philosophical Transactions of the Royal Society A*, *374*(20140297), 1–21. https://doi.org/10.1098/rsta.2014.0297

Young, D. A., Blankenship, D. D., Kempf, S. D., Quartini, E., Muldoon, G. R., & Powell, E. M. (2017). *Ice thickness and related data over central Marie Byrd Land, West Antarctica (GIMBLE.GR2HI2)*. U.S. Antarctic Program (USAP) Data Center. https://doi.org/10.15784/601001